

Intrinsic Gyrotropic Magnetic Current of Orbital Origin

Koushik Ghorai,* Sankar Sarkar,† and Amit Agarwal‡

Department of Physics, Indian Institute of Technology Kanpur, Kanpur-208016, India

In gyrotropic crystals, an oscillating magnetic field induces a charge response known as the gyrotropic magnetic current. While its conventional origin is attributed to magnetic field modified band energy and shift in the Fermi-surface, a recent study identified an additional spin-driven magnetic displacement contribution. Here, we complete the picture by identifying the orbital counterpart of the magnetic displacement current. Using a density-matrix formulation that incorporates both minimal coupling and spin-Zeeman interactions, we derive the electronic equations of motion in the presence of an oscillating magnetic field and uncover a previously unexplored orbital contribution to the wavepacket velocity. Physically, this contribution arises from the time variation of the magnetic field induced charge polarization. In the low frequency transport regime, this mechanism becomes purely intrinsic. We illustrate this intrinsic gyrotropic current of orbital origin in the \mathcal{PT} -symmetric antiferromagnet CuMnAs. We show that the intrinsic gyrotropic magnetic current reverses sign upon Néel vector reversal, establishing it as a direct probe of antiferromagnetic order in CuMnAs and other \mathcal{PT} -symmetric antiferromagnets.

I. INTRODUCTION

The gyrotropic effect typically refers to the generation of an axial (polar) response for a polar (axial) driving field. It includes a variety of phenomena such as optical activity^{1–3}, circular dichroism⁴, Faraday rotation, circular photogalvanic effect⁵, magnetoelectric effect^{6–8}, and gyrotropic Hall effect⁹ amongst others. A particularly intriguing effect is the gyrotropic magnetic current (GMC), where a slowly varying magnetic field drives a dissipationless electrical current. GMC in metals was first identified by Zhong *et al.* as a low-frequency limit of optical gyrotropy¹⁰. It has been explored in Weyl semimetals¹¹ and chiral magnets¹². Since GMC arises from the magnetic moments of quasiparticles near the Fermi surface, it has become a sensitive probe of materials' symmetry, Berry curvature, degeneracy of chiral fermions, and band geometric quantities^{13–17}.

Microscopically, GMC originates from intrinsic and disorder-induced corrections to the electronic magnetic moment¹⁸. Recent works have pointed out that beyond the Zeeman-coupling induced modification of band energies, magnetic driving induces a positional shift of the electronic wavepacket, leading to a finite charge polarization^{19,20}. For an oscillating magnetic field, the temporal modulation of this polarization generates a magnetic analogue of the electric field induced displacement current^{21,22}. Recently, Wang *et al.*²³ identified the spin contribution to this magnetic displacement current and demonstrated that it constitutes an intrinsic gyrotropic magnetic current (IGMC) at finite frequency. However, the corresponding orbital contribution was not addressed. This omission is particularly significant in view of growing evidence that orbital mechanisms dominate a wide range of responses in weak spin-orbit coupled materials^{24–31}. Orbital effects have also been shown to generate additional contributions to electronic charge transport^{14,32–35}.

In this work, we develop a unified theory of IGMC that treats spin and orbital coupling on an equal foot-

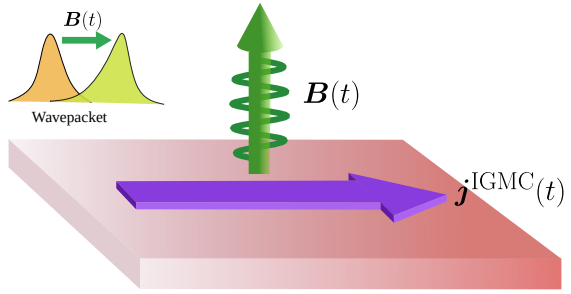


FIG. 1. Schematic of the intrinsic gyrotropic magnetic current (IGMC) of orbital origin. A time-varying magnetic field $\mathbf{B}(t)$ couples to the electronic orbital magnetic moment, inducing an orbital contribution to the oscillatory positional shift of the wave packet and dynamic charge polarization. The time variation of this polarization gives rise to the IGMC response.

ing. Starting from a density-matrix framework, we derive the semiclassical, finite-frequency equations of motion (EOM) of electron wavepackets in the presence of an oscillating magnetic field. This enables us to identify the previously overlooked orbital contribution to IGMC arising from the orbital-induced positional shift of the Bloch electrons. We quantify this positional shift, or the Berry connection correction, by introducing a band geometric quantity: *orbital*-magnetic Berry connection polarizability (MBCP). Its spin counterpart is denoted as *spin*-MBCP. Importantly, this density matrix formulation of Berry connection correction contains an extra multiband term in MBCP that was missing in earlier semiclassical treatments^{19,30}.

In contrast to the Fermi surface nature of conventional GMC, IGMC is a Fermi sea response, and it is finite in both metals and in insulators. Another interesting distinction between them is that while IGMC is symmetry allowed and becomes the leading gyrotropic response in systems with combined inversion (\mathcal{P}) and time-reversal (\mathcal{T}) symmetry (bipartite antiferromagnets), conventional

GMC is restricted in such systems by symmetry. We further analyze the crystallographic point group symmetry of the IGMC response tensors to facilitate the right material selection. Owing to this, we demonstrate the orbital-driven IGMC in \mathcal{PT} -symmetric antiferromagnetic phase of tetragonal CuMnAs. Notably, the orbital mechanism of IGMC dominates the response and is almost an order of magnitude larger than its spin counterpart in CuMnAs. Being a time-reversal-odd response, IGMC shows a distinct signature in CuMnAs: it reverses sign as the magnetization order, or the Néel vector, is reversed. This establishes IGMC as an interesting mechanism to probe the antiferromagnetic ordering.

The rest of the paper is organized as follows: Section II develops the density matrix formulation of the finite frequency EOM. Section III presents different contributions to IGMC, including the novel contribution due to the orbital part of the magnetic displacement current. We discuss the fundamental and crystallographic point group symmetry restrictions of the IGMC responses in Section IV. We demonstrate the IMGC response in anti-ferromagnetic CuMnAs in Section V. In Section VI, we summarize our main findings.

II. DENSITY MATRIX FORMULATION OF EQUATION OF MOTION

In this section, we derive the electronic EOM in the presence of a harmonically oscillating magnetic field of amplitude \mathbf{B}_0 and frequency ω ,

$$\mathbf{B}(t) = \frac{1}{2}\mathbf{B}_0 e^{i\omega t} + \text{c.c.} \quad (1)$$

We derive the semiclassical dynamics of Bloch electrons in crystalline materials using the Euler-Lagrange formalism. Semiclassically, the Lagrangian is obtained by taking the expectation value of the Lagrangian operator $\hat{\mathcal{L}} = i\hbar\partial_t - \hat{\mathcal{H}}$ over the electronic wavepacket $|W\rangle$,

$$\mathcal{L} = \langle W | i\hbar \frac{\partial}{\partial t} - \hat{\mathcal{H}} | W \rangle. \quad (2)$$

Here, $\hat{\mathcal{H}} = \hat{\mathcal{H}}_0 + \hat{\mathcal{H}}^B$ is the total Hamiltonian with an unperturbed $\hat{\mathcal{H}}_0$ and the magnetic interaction term $\hat{\mathcal{H}}^B$. In this work, we consider the magnetic coupling with both orbital and spin magnetic moments, giving rise to the total magnetic perturbation

$$\hat{\mathcal{H}}^B = \hat{\mathcal{H}}_L^B + \hat{\mathcal{H}}_S^B = -\mathbf{B} \cdot \hat{\mathbf{M}}^L - \mathbf{B} \cdot \hat{\mathbf{M}}^S. \quad (3)$$

Here, $\hat{\mathbf{M}}^L = -(e/4)[\hat{\mathbf{r}} \times \hat{\mathbf{v}} - \hat{\mathbf{v}} \times \hat{\mathbf{r}}]$ is the orbital magnetic-moment operator, and $\hat{\mathbf{M}}^S = -(g_s\mu_B/2)\hat{\boldsymbol{\sigma}}$ is its spin counterpart. Here, $\hat{\mathbf{r}}$ and $\hat{\mathbf{v}}$ refers to the electronic position and velocity operators, respectively, $g_s \simeq 2$ is the spin g -factor, μ_B denotes the Bohr magneton, and $\hat{\boldsymbol{\sigma}}$ corresponds to the Pauli matrices.

Instead of following the conventional wavepacket formalism^{20,36}, here we employ a density-matrix approach³⁷ to construct the Lagrangian. The advantage of this formulation is twofold: first, it unifies these two frameworks

under dynamic magnetic perturbation; second, the finite frequency density matrix solution can be employed in other magnetotransport studies. In the density matrix formulation, the system Lagrangian is defined as the trace of the Lagrangian operator $\hat{\mathcal{L}}$ weighted by the density matrix $\hat{\rho}$,

$$\mathcal{L} = \text{Tr}\{\hat{\mathcal{L}}\hat{\rho}\}. \quad (4)$$

In the presence of a magnetic field, the evolution of the density matrix is described by the quantum Liouville equation³⁸. We have,

$$\frac{\partial \hat{\rho}}{\partial t} + \frac{i}{\hbar} [\hat{\mathcal{H}}_0, \hat{\rho}] + \frac{1}{\tau} \hat{\rho} = \mathcal{D}_B \hat{\rho} - \frac{i g_s \mu_B}{2\hbar} \mathbf{B} \cdot [\hat{\boldsymbol{\sigma}}, \hat{\rho}], \quad (5)$$

where τ denotes the scattering time that captures the relaxation of the electronic states of the system. The first term on the right-hand side describes the coupling between the magnetic field and the orbital motion of Bloch electrons, while the second represents the Zeeman coupling to spin. The explicit form of the orbital contribution is given by

$$[\mathcal{D}_B \hat{\rho}]_{nm} = \frac{e}{2\hbar^2} B_0^c \epsilon_{cab} \left\{ \mathcal{D}_b \hat{\mathcal{H}}_0, \mathcal{D}_a \hat{\rho} \right\}_{nm}, \quad (6)$$

where $\{a, b, c\}$ denote Cartesian components, and summation over repeated indices is implied. The action of the covariant derivative³⁹ in momentum space on an operator $\hat{\mathcal{X}}$ is given by

$$[\mathcal{D}_{\mathbf{k}} \hat{\mathcal{X}}]_{nm} \equiv \left(\frac{\mathcal{D} \hat{\mathcal{X}}}{\mathcal{D} \mathbf{k}} \right)_{nm} = \partial_{\mathbf{k}} \mathcal{X}_{nm} - i[\hat{\mathcal{R}}, \hat{\mathcal{X}}]_{nm}. \quad (7)$$

Here, $[\hat{\mathcal{R}}]_{nm} \equiv \mathcal{R}_{nm} = \langle u_{n\mathbf{k}} | i\partial_{\mathbf{k}} | u_{m\mathbf{k}} \rangle$ is the band-resolved Berry connection, and $|u_{n\mathbf{k}}\rangle$ is the cell-periodic part of the Bloch eigenstates $|\psi_{n\mathbf{k}}\rangle = e^{i\mathbf{k}\cdot\mathbf{r}} |u_{n\mathbf{k}}\rangle$ for an n^{th} band electron with momentum \mathbf{k} and eigenvalue $\varepsilon_{n\mathbf{k}}$. The spin part of the magnetic interaction is captured by the second term on the right-hand side in Eq. (5).

In the weak field limit, we solve Eq. (5) perturbatively to obtain the density matrix elements at different orders in magnetic field strength. The first-order solution of the density matrix is expressed as,

$$\rho_{nm}^B(t) = \rho_{nm}^B(\omega) e^{i\omega t} + \rho_{nm}^B(-\omega) e^{-i\omega t}. \quad (8)$$

The harmonic components of the density matrix can be segregated into an orbital ($\rho_{nm;L}^B$) and a spin part ($\rho_{nm;S}^B$),

$$\rho_{nm}^B(\omega) = \rho_{nm;L}^B(\omega) + \rho_{nm;S}^B(\omega). \quad (9)$$

We calculate these terms explicitly in Appendix. A to obtain,

$$\rho_{nm;S}^B(\omega) = \frac{i g_s \mu_B}{4\hbar} g_{nm}^{\omega} [\mathbf{B}_0 \cdot \boldsymbol{\sigma}_{nm}] f_{nm}, \quad (10)$$

and

$$\rho_{nm;L}^B(\omega) = \frac{e}{4\hbar}g_{nm}^\omega \mathbf{B}_0 \cdot [\{\partial_{\mathbf{k}}(f_n + f_m)\} \times \mathbf{v}_{nm}] + \frac{i}{2\hbar}g_{nm}^\omega \mathbf{B}_0 \cdot \sum_{p \neq m} \left[\mathcal{M}_{npm}^L f_{pm} - \left(\mathcal{M}_{mpn}^L \right)^* f_{pn} \right]. \quad (11)$$

Here $g_{nm}^\omega = [1/\tau + i(\omega_{nm} + \omega)]^{-1}$ with $\hbar\omega_{nm} = \varepsilon_{n\mathbf{k}} - \varepsilon_{m\mathbf{k}}$ being interband transition frequency. Additionally, $f_{pm} = (f_p - f_m)$ is the equilibrium population difference, $\mathcal{M}_{mpn}^L = -(e/2)(\mathbf{v}_{mp} + \delta_{mp}\mathbf{v}_n) \times \mathcal{R}_{pn}$, and $\mathbf{v}_{nm} = (1/\hbar)\langle u_{n\mathbf{k}} | \partial_{\mathbf{k}} \mathcal{H}_0 | u_{m\mathbf{k}} \rangle$ corresponds to the unperturbed velocity matrix element. We substitute this density matrix in Eq. (4) to obtain the n^{th} band Lagrangian,

$$\mathcal{L}_{n\mathbf{k}} = -\hbar\dot{\mathbf{k}} \cdot (\mathbf{r}_n - \tilde{\mathcal{R}}_{n\mathbf{k}}) + \frac{e}{2}(\mathbf{B} \times \dot{\mathbf{r}}_n) \cdot \mathbf{r}_n - \tilde{\varepsilon}_{n\mathbf{k}}, \quad (12)$$

where \mathbf{r}_n is the average electronic position in a unit cell, or, equivalently, the center of a semiclassical wavepacket. $\tilde{\mathcal{R}}_{n\mathbf{k}} = \mathcal{R}_{n\mathbf{k}} + \mathcal{R}_{n\mathbf{k}}^B(t)$ is the magnetic field induced total Berry connection, and $\tilde{\varepsilon}_{n\mathbf{k}} = \varepsilon_{n\mathbf{k}} - (\mathcal{M}_{n\mathbf{k}}^L + \mathcal{M}_{n\mathbf{k}}^S) \cdot \mathbf{B}$ corresponds to the field-corrected band energy. The details of the calculation are presented in Appendix B.

The Berry connection correction $\mathcal{R}_{n\mathbf{k}}^B(t)$ emerges due to the magnetic field driven shift in charge distribution and can be expressed in the following form

$$\mathcal{R}_{n\mathbf{k}}^{B;a}(t) = \tilde{\mathcal{G}}_{n\mathbf{k}}^{B;ad}(\omega)B_0^d e^{i\omega t} + \text{c.c.} \quad (13)$$

Here, we have introduced a band-geometric quantity $\tilde{\mathcal{G}}_{n\mathbf{k}}^{B;ad}(\omega)$ and we term it as magnetic Berry connection

$$\tilde{\mathcal{G}}_{n\mathbf{k};L}^{B;ad}(\omega) = -\frac{e}{4\hbar} \sum_{m \neq n} \epsilon_{dbc} \partial_b \left[g_{nm}^\omega v_{nm}^c \mathcal{R}_{mn}^a \right] - \frac{i}{2\hbar} \sum_{m \neq n} g_{mn}^\omega \mathcal{M}_{mn}^{L;d} \mathcal{R}_{nm}^a + \frac{i}{2\hbar} \sum_{m \neq p} \sum_{p \neq n} g_{mp}^\omega \mathcal{M}_{mpn}^{L;d} \mathcal{R}_{pm}^a. \quad (17)$$

Here, $\mathcal{M}_{mn}^L = \sum_{p \neq n} \mathcal{M}_{mpn}^L$ is the matrix element of the orbital magnetic moment operator. The *spin*-MBCP has been explored in some recent articles^{23,42,43} and it is also referred to as anomalous spin polarizability⁴⁴. The *orbital*-MBCP emerges naturally from the present formulation. The first two terms in Eq. (17) generalize the earlier result of the orbital contribution to the magnetic field induced Berry connection^{44,45} to include finite frequency and disorder effects (See Appendix B for details). Additionally, the last term in Eq. (17) captures a unique multiband contribution to the MBCP that has not been explored earlier.

In two-dimensional materials, the out-of-plane orbital magnetic moment can couple to only an out-of-plane magnetic field. Thereby, *orbital*-MBCP would vanish for an in-plane magnetic field. However, the *spin*-MBCP may survive in such a scenario. More importantly, the time-dependent Berry connection remains gauge-invariant, similar to its dc counterpart.

polarizability (MBCP). Similar to the electric field induced Berry connection polarizability^{19,40,41}, the magnetic field driven correction is also a result of field induced interband transitions or mixing of Bloch states and would vanish if the magnetic driving is switched off ($\mathbf{B} \rightarrow 0$). Since the interband hybridization can be generated by both minimal coupling perturbation and Zeeman interaction, both orbital and spin magnetic moments would contribute to the Berry connection correction. Accordingly, we split finite-frequency MBCP into a spin and an orbital part,

$$\tilde{\mathcal{G}}_{n\mathbf{k}}^{B;ad}(\omega) = \tilde{\mathcal{G}}_{n\mathbf{k};S}^{B;ad}(\omega) + \tilde{\mathcal{G}}_{n\mathbf{k};L}^{B;ad}(\omega). \quad (14)$$

The *spin*-MBCP ($\tilde{\mathcal{G}}_{n;S}^{B;ad}$) and *orbital*-MBCP ($\tilde{\mathcal{G}}_{n;L}^{B;ad}$) are defined as follows:

$$\tilde{\mathcal{G}}_{n\mathbf{k};S/L}^{B;ad}(\omega) = \mathcal{G}_{n\mathbf{k};S/L}^{B;ad}(\omega) + \left[\mathcal{G}_{n\mathbf{k};S/L}^{B;ad}(-\omega) \right]^*, \quad (15)$$

where

$$\mathcal{G}_{n\mathbf{k};S}^{B;ad}(\omega) = \frac{i}{2\hbar} \sum_{m \neq n} g_{mn}^\omega \mathcal{M}_{mn}^{S;d} \mathcal{R}_{nm}^a, \quad (16)$$

and

A. Equation of Motion

The dynamics of Bloch electrons can be obtained from the derived Lagrangian in Eq. (12) using Euler-Lagrange equations

$$\frac{d}{dt} \left(\frac{\partial \mathcal{L}_{n\mathbf{k}}}{\partial \dot{\mathbf{k}}} \right) = \frac{\partial \mathcal{L}_{n\mathbf{k}}}{\partial \mathbf{k}}, \quad (18)$$

$$\frac{d}{dt} \left(\frac{\partial \mathcal{L}_{n\mathbf{k}}}{\partial \dot{\mathbf{r}}_{n\mathbf{k}}} \right) = \frac{\partial \mathcal{L}_{n\mathbf{k}}}{\partial \mathbf{r}_{n\mathbf{k}}}. \quad (19)$$

The first Euler-Lagrange equation yields the quasiparticle velocity

$$\dot{\mathbf{r}}_{n\mathbf{k}} = \tilde{\mathbf{v}}_{n\mathbf{k}} - \dot{\mathbf{k}} \times (\mathbf{\Omega}_{n\mathbf{k}} + \mathbf{\Omega}_{n\mathbf{k}}^B) + \frac{\partial \mathcal{R}_{n\mathbf{k}}^B}{\partial t}. \quad (20)$$

Here, $\tilde{\mathbf{v}}_{n\mathbf{k}} = (1/\hbar)\partial_{\mathbf{k}}\tilde{\varepsilon}_{n\mathbf{k}}$ is the magnetic field corrected band velocity and $\mathbf{\Omega}_{n\mathbf{k}}(\mathbf{\Omega}_{n\mathbf{k}}^B) = \partial_{\mathbf{k}} \times \mathcal{R}_{n\mathbf{k}}(\mathcal{R}_{n\mathbf{k}}^B)$ is the unperturbed (magnetic field induced) Berry curvature of

the system. The second Euler-Lagrange equation produces the familiar force equation,

$$\hbar \dot{\mathbf{k}} = -e[\mathbf{\dot{r}}_{n\mathbf{k}} \times \mathbf{B}(t)]. \quad (21)$$

These equations of motion can be decoupled to obtain,

$$\mathbf{\dot{r}}_{n\mathbf{k}} = D_{n\mathbf{k}} \left[\tilde{\mathbf{v}}_{n\mathbf{k}} + \frac{e}{\hbar} (\mathbf{v}_{n\mathbf{k}} \cdot \boldsymbol{\Omega}_{n\mathbf{k}}) \mathbf{B} + \frac{\partial \mathcal{R}_{n\mathbf{k}}^B}{\partial t} \right], \quad (22)$$

$$\hbar \dot{\mathbf{k}} = D_{n\mathbf{k}} [-e(\mathbf{v}_{n\mathbf{k}} \times \mathbf{B})], \quad (23)$$

where $D_{n\mathbf{k}} = [1 + e/\hbar(\mathbf{B} \cdot \tilde{\boldsymbol{\Omega}}_{n\mathbf{k}})]^{-1}$ is the semiclassical phase space factor⁴⁶. The detailed derivation of EOM is presented in Appendix C. In Eq. (22), the first term corresponds to the field-modified band velocity, the second term is the ‘chiral magnetic velocity’ (CMV)⁴⁷ that gives rise to the chiral magnetic effect and the chiral anomaly⁴⁸ induced negative magneto-resistance in three-dimensional Weyl semimetals^{49,50}. The third contribution is new and arises from the magnetic field perturbed wavefunction. It contains both spin and orbital components. While the spin part of the third term was discussed recently by Wang *et al.*²³, its orbital counterpart has not been reported before. Importantly, this velocity component, being the time derivative of the field-corrected Berry connection, contributes only in the presence of a dynamic magnetic field and vanishes for static driving. Additionally, in two-dimensional materials, the chiral velocity term vanishes due to the orthogonal configuration of electronic velocity and Berry curvature.

III. GYROTROPIC MAGNETIC CURRENT

In the last section, we derived the particle velocity in the presence of an oscillating magnetic field. This velocity weighted by the nonequilibrium distribution function and the phase space correction factor, yields the charge current

$$\mathbf{j} = -e \int_{n\mathbf{k}} D_{n\mathbf{k}}^{-1} \mathbf{\dot{r}}_{n\mathbf{k}} \tilde{f}_{n\mathbf{k}}. \quad (24)$$

For simplicity, we have defined $\int_{n\mathbf{k}} \equiv \sum_n \int d^d \mathbf{k} / (2\pi)^d$, with d being the spatial dimension of the system. For a spatially homogeneous perturbation, the field-modified electronic distribution function $\tilde{f}_{n\mathbf{k}}$ is obtained by solving the Boltzmann equation under relaxation time approximation⁵¹,

$$\frac{\partial \tilde{f}_{n\mathbf{k}}}{\partial t} + \dot{\mathbf{k}} \cdot \nabla_{\mathbf{k}} \tilde{f}_{n\mathbf{k}} = -\frac{\tilde{f}_{n\mathbf{k}} - f_{n\mathbf{k}}^B}{\tau}. \quad (25)$$

Here, $f_{n\mathbf{k}}^B = (1 + e^{\beta(\tilde{\varepsilon}_{n\mathbf{k}} - \mu)})^{-1}$ is the Fermi-Dirac distribution function of the magnetic field perturbed band $\tilde{\varepsilon}_{n\mathbf{k}}$ with chemical potential μ and inverse temperature $\beta = 1/(k_B T)$. Due to periodic magnetic driving, the nonequilibrium correction part $\delta f_{n\mathbf{k}} = \tilde{f}_{n\mathbf{k}} - f_{n\mathbf{k}}^B$ would be in harmonics of the driving field. Solving Eq. (25)

up to the linear order of the field, we obtain $\delta f_{n\mathbf{k}}(t) = \delta f_{n\mathbf{k}}(\omega) e^{i\omega t} + \text{c.c.}$, with

$$\delta f_{n\mathbf{k}}(\omega) = i\omega g_0^\omega (\mathbf{M}_{n\mathbf{k}} \cdot \mathbf{B}_0) \frac{\partial f_{n\mathbf{k}}}{\partial \varepsilon_{n\mathbf{k}}}, \quad (26)$$

where $g_0^\omega = [1/\tau + i\omega]^{-1}$, and $f_{n\mathbf{k}}$ corresponds to the equilibrium Fermi function without any magnetic field. Substitution of the field induced distribution function and the particle velocity from Eq. (22) into Eq. (24) and keeping terms only up to first order in the magnetic field yields the linear gyrotropic current. We express it as

$$j_a^{\text{GMC}}(t) = \chi_{a;d}^{\text{GMC}}(\omega) B_0^d e^{i\omega t} + \text{c.c.}, \quad (27)$$

where $\{a, d\}$ refer to cartesian indices. The gyrotropic magnetic conductivity $\chi_{a;d}^{\text{GMC}}(\omega)$ originates from three different physical processes: Fermi-surface oscillation, dynamic charge polarization, and chiral magnetic velocity. This allows us to express the gyromagnetic response as,

$$\chi_{a;d}^{\text{GMC}}(\omega) = \chi_{a;d}^{\text{G,FO}} + \chi_{a;d}^{\text{G,Disp}} + \chi_{a;d}^{\text{G,CMV}}. \quad (28)$$

The Fermi surface oscillation term $\chi_{a;d}^{\text{G,FO}}$ arises from the nonequilibrium distribution function and corresponds to the conventional gyrotropic current¹⁰

$$\chi_{a;d}^{\text{G,FO}}(\omega) = -ie\omega g_0^\omega \int_{n\mathbf{k}} v_{n\mathbf{k}}^a \mathbf{M}_{n\mathbf{k}}^d \frac{\partial f_{n\mathbf{k}}}{\partial \varepsilon_{n\mathbf{k}}}, \quad (29)$$

where $\mathbf{M}_{n\mathbf{k}} = (\mathbf{M}_{n\mathbf{k}}^L + \mathbf{M}_{n\mathbf{k}}^S)$ denotes the momentum resolved total magnetic moment.

The displacement contribution, $\chi_{a;d}^{\text{G,Disp}}$, originates from a magnetic field induced dynamic charge polarization,

$$P_a(t) = -e \int_{n\mathbf{k}} \mathcal{R}_{n\mathbf{k}}^{B;a}(t) f_{n\mathbf{k}} = \mu_{a;d}(\omega) B_0^d e^{i\omega t} + \text{c.c.} \quad (30)$$

Here, $\mu_{a;d}(\omega)$ corresponds to the ‘magnetic polarizability’,

$$\mu_{a;d}(\omega) = -e \int_{n\mathbf{k}} \tilde{\mathcal{G}}_{n\mathbf{k}}^{B;ad}(\omega) f_{n\mathbf{k}}. \quad (31)$$

The temporal variation of the charge polarization generates a gyrotropic magnetic displacement current $\partial \mathbf{P} / \partial t$. The corresponding gyrotropic conductivity is given by

$$\chi_{a;d}^{\text{G,Disp}}(\omega) = -ie\omega \int_{n\mathbf{k}} \tilde{\mathcal{G}}_{n\mathbf{k}}^{B;ad}(\omega) f_{n\mathbf{k}}. \quad (32)$$

Importantly, the gyrotropic conductivity is related to the ‘magnetic polarizability’ through $\chi_{a;d}^{\text{G,Disp}}(\omega) = i\omega \mu_{a;d}(\omega)$, providing a direct probe of the system’s polarization response to magnetic driving. This is one of the central results in this paper and constitutes a novel addition to the GMC.

TABLE I. The symmetry restrictions and physical origin of different contributions to the intrinsic gyrotropic magnetic current. The integrands of the current components are summed over all bands (n) and integrated over momentum (\mathbf{k}) space. This combined operation is denoted by $\int_{n\mathbf{k}} \equiv \sum_n \int d^d\mathbf{k}/(2\pi)^d$, where d is the spatial dimension of the system. Here, \mathcal{P} and \mathcal{T} (\mathcal{P} , \mathcal{T}) indicate that spatial inversion and time-reversal symmetries are broken (preserved) in the system. The cross (\times) and the tick (\checkmark) mark signify that the corresponding response tensor is symmetry forbidden and allowed, respectively.

Conductivity	Expression	\mathcal{P}, \mathcal{T}	\mathcal{P}, \mathcal{T}	\mathcal{P}, \mathcal{T}	\mathcal{P}, \mathcal{T}	Physical Origin
$\chi_{a;d}^{\text{IG,Disp}}$	$-ie\omega \int_{n\mathbf{k}} \tilde{\mathcal{G}}_n^{B;ad}(\omega) f_{n\mathbf{k}}$	\times	\times	\checkmark	\checkmark	$\mathbf{B}(t)$ -induced Polarization Oscillation
$\chi_{a;d}^{\text{G,CMV}}$	$-\delta_{ad}(e^2/\hbar) \int_{n\mathbf{k}} (\mathbf{v}_{n\mathbf{k}} \cdot \boldsymbol{\Omega}_{n\mathbf{k}}) f_{n\mathbf{k}}$	\times	\checkmark	\checkmark	\times	Chiral Magnetic Velocity

The third term, $\chi_{a;d}^{\text{G,CMV}}$, stems from the CMV

$$\chi_{a;d}^{\text{G,CMV}}(\omega) = -\frac{e^2}{\hbar} \delta_{ad} \int_{n\mathbf{k}} (\mathbf{v}_{n\mathbf{k}} \cdot \boldsymbol{\Omega}_{n\mathbf{k}}) f_{n\mathbf{k}}. \quad (33)$$

It drives a current strictly along the direction of the magnetic field.

In addition to their physical origin, these components also differ in other aspects. Both $\chi_{a;d}^{\text{G,FO}}$ and $\chi_{a;d}^{\text{G,Disp}}$ are purely dynamic and vanish in the dc limit ($\omega \rightarrow 0$), whereas $\chi_{a;d}^{\text{G,CMV}}$ can persist even for static fields. However, for static driving, the CMV-induced current or the chiral magnetic effect^{52,53}, requires the system to be in an initial nonequilibrium state^{54,55}. Even for a dynamical magnetic field, this current survives only in the presence of a chiral chemical imbalance⁵⁶, typically observed in inversion-broken Weyl semimetal^{11,57}, and vanishes in other materials. Another differentiating aspect of the three contributions of GMC is that $\chi_{a;d}^{\text{G,FO}}$ is a Fermi-surface response and finite only in metals or doped semiconductors. In contrast, the chiral magnetic part originates from the Fermi sea, and the displacement term contains both Fermi-surface and Fermi-sea contributions. Consequently, they enable finite gyrotropic responses even in insulating systems. In addition, the three conductivity components obey distinct symmetry constraints, which are discussed in Sec. IV.

We next focus on the intrinsic component of the GMC. The chiral-current contribution is purely intrinsic, while the conventional and displacement currents depend explicitly on the symmetric scattering time τ . The τ -dependence of the conventional term originates from g_0^ω , whereas in the displacement current it arises from $g_{nm}^\omega = [1/\tau + i(\omega_{nm} + \omega)]^{-1}$. In the transport regime ($\omega\tau \ll 1$), these factors approximate to $g_0^\omega \approx \tau$ and $g_{nm}^\omega \approx [i(\omega_{nm} + \omega)]^{-1}$. As a consequence, in this regime, the conventional GMC becomes purely extrinsic while the displacement contribution is an intrinsic response governed solely by the band-geometric MBCP tensor. We express the total intrinsic gyrotropic magnetic current (IGMC) as

$$j_a^{\text{IGMC}}(t) = \chi_{a;d}^{\text{IGMC}}(\omega) B_0^d e^{i\omega t} + \text{c.c.}, \quad (34)$$

where the corresponding conductivity is given by

$$\chi_{a;d}^{\text{IGMC}}(\omega) = \chi_{a;d}^{\text{IG,Disp}} + \chi_{a;d}^{\text{G,CMV}}. \quad (35)$$

The expressions of these contributions to the IGMC, together with their contrasting fundamental symmetry restrictions, are summarized in Table I. The detailed calculation of IGMC is presented in Appendix D.

IV. SYMMETRY ANALYSIS

In this section, we analyze the symmetry properties of the intrinsic gyrotropic magnetic current. Having established the distinct microscopic origins of the individual IGMC channels, we first examine how the underlying band-geometric quantities transform under fundamental symmetry operations. This allows us to identify the channel-resolved symmetry restrictions governing the displacement, and chiral contributions to IGMC, and to distinguish which mechanisms can contribute in different symmetry classes of materials.

Under spatial inversion (\mathcal{P}), the electrical current reverses sign, $\mathbf{j} \rightarrow -\mathbf{j}$, while the magnetic field remains invariant, $\mathbf{B} \rightarrow \mathbf{B}$. Invariance of the linear response relation in Eq. (34) therefore requires the gyrotropic magnetic conductivity tensor $\chi_{a;d}^{\text{IGMC}}$ to change sign under \mathcal{P} . However, because conductivity is an intrinsic material property, it must remain invariant in a centrosymmetric crystal. As a consequence, a nonzero IGMC is symmetry allowed only in inversion-broken, i.e., noncentrosymmetric, systems. Under time-reversal symmetry (\mathcal{T}), both the current and the magnetic field reverse sign, $\mathbf{j} \rightarrow -\mathbf{j}$ and $\mathbf{B} \rightarrow -\mathbf{B}$, leaving the overall IGMC response invariant. The gyrotropic magnetic current is therefore not prohibited by time-reversal symmetry and can arise in

TABLE II. The symmetry transformations of the band geometric quantities in momentum space under inversion (\mathcal{P}), time-reversal (\mathcal{T}) and combined parity-time reversal (\mathcal{PT}) operation.

Quantity	\mathcal{P}	\mathcal{T}	\mathcal{PT}
$\mathcal{R}_{nm}(\mathbf{k})$	$-\mathcal{R}_{nm}(-\mathbf{k})$	$\mathcal{R}_{mn}(-\mathbf{k})$	$-\mathcal{R}_{mn}(-\mathbf{k})$
$\mathbf{v}_{nm}(\mathbf{k})$	$-\mathbf{v}_{nm}(-\mathbf{k})$	$-\mathbf{v}_{mn}(-\mathbf{k})$	$\mathbf{v}_{mn}(-\mathbf{k})$
$\boldsymbol{\mathcal{M}}_{nm}(\mathbf{k})$	$\boldsymbol{\mathcal{M}}_{nm}(-\mathbf{k})$	$-\boldsymbol{\mathcal{M}}_{mn}(-\mathbf{k})$	$-\boldsymbol{\mathcal{M}}_{mn}(\mathbf{k})$

TABLE III. The symmetry restrictions of the magnetic gyrotropic response tensors. The cross (\times) and the tick (\checkmark) mark signify that the corresponding response tensor is symmetry forbidden and allowed, respectively. Here, \mathcal{M}_a , \mathcal{C}_n^a and \mathcal{S}_n^a ($\mathcal{C}_n^a \mathcal{M}_a$) represent mirror, n -fold rotation, and n -fold roto-reflection symmetry operation along the a -direction for $a = \{x, y, z\}$, respectively.

IGMC	\mathcal{M}_x	\mathcal{M}_y	\mathcal{M}_z	\mathcal{C}_n^x	\mathcal{C}_n^y	\mathcal{C}_n^z	\mathcal{S}_4^x	\mathcal{S}_4^y	\mathcal{S}_4^z	\mathcal{S}_6^a
$\chi_{x;z}^{\text{IGMC}}$	\checkmark	\times	\checkmark	\times	\checkmark	\times	\times	\checkmark	\times	\times
$\chi_{y;z}^{\text{IGMC}}$	\times	\checkmark	\checkmark	\checkmark	\times	\times	\checkmark	\times	\times	\times

both magnetic and nonmagnetic materials.

While this establishes the general conditions for a nonvanishing IGMC, it does not specify which of the underlying microscopic mechanisms, namely, the magnetic displacement current and the chiral magnetic velocity, can contribute in a given material. To address this question, we examine the momentum-space parity of the conductivity integrands associated with the relevant band-geometric quantities. Using the transformation properties summarized in Table II, we find that in inversion-broken nonmagnetic crystals, the chiral channel is symmetry allowed, whereas the displacement contribution vanishes. In contrast, in \mathcal{PT} -symmetric systems, the chiral component is forbidden, leaving a purely displacement current driven intrinsic gyrotropic magnetic response.

Having established the fundamental symmetry properties of the individual IGMC channels, we now examine the additional constraints imposed by crystallographic point group operations. The transformation behavior of a linear response tensor under a point group operation is dictated by two attributes: (i) whether the tensor is polar or axial, and (ii) its time-reversal parity. From Eq. (34), which relates the polar current vector \mathbf{j} to the axial magnetic field \mathbf{B} , it follows that the gyrotropic magnetic conductivity $\chi_{a;d}^{\text{IGMC}}$ is a second-rank axial tensor⁵⁸.

Among the two contributions to IGMC, the chiral magnetic velocity term $\chi_{a;d}^{\text{IG,CMV}}$ is even under time-reversal symmetry. In contrast, the displacement current contribution $\chi_{a;d}^{\text{IG,Disp}}$ is odd under time-reversal. For a general crystallographic point group operation \mathcal{O} , these tensors transform as

$$\chi_{a';d'}^{\text{IG,CMV}} = \det\{\mathcal{O}\} \mathcal{O}_{a'a} \mathcal{O}_{d'd} \chi_{a;d}^{\text{IG,CMV}}, \quad (36)$$

$$\chi_{a';d'}^{\text{IG,Disp}} = \eta_{\mathcal{T}} \det\{\mathcal{O}\} \mathcal{O}_{a'a} \mathcal{O}_{d'd} \chi_{a;d}^{\text{IG,Disp}}. \quad (37)$$

Here, $\eta_{\mathcal{T}} = +1$ for purely spatial operations ($\mathcal{O} = R$) and $\eta_{\mathcal{T}} = -1$ for magnetic operations involving time-reversal ($\mathcal{O} = R\mathcal{T}$). Since the \mathcal{T} -even and \mathcal{T} -odd parts of IGMC response tensors transform identically under nonmagnetic point group operations, they obey the same symmetry constraints in this case. Accordingly, rather than listing separate symmetry tables for each contribution, we present the allowed components of the total

IGMC tensor in Table III. For magnetic point groups, however, the two sectors transform differently and must be treated separately. The corresponding symmetry conditions for $\chi_{a;d}^{\text{IG,CMV}}$ and $\chi_{a;d}^{\text{IG,Disp}}$ are summarized in Table IV of Appendix E.

V. IGMC IN CuMnAs

In tetragonal CuMnAs^{59,60}, the Mn atoms form two interpenetrating antiferromagnetic sublattices (denoted by Mn_A and Mn_B) as shown in Fig. 2(a). These magnetic atoms experience locally broken inversion symmetry, while being related to each other by the combined \mathcal{PT} operation. The asymmetric local environment manifests via a sublattice-dependent anisotropic Rashba spin-orbit coupling (SOC). Due to the antiferromagnetic arrangement, the staggered magnetic moments are also subjected to a sublattice-contrasting exchange energy. Incorporating these energy contributions along with the intra- and inter-sublattice hopping, the minimal tight-binding Hamiltonian of CuMnAs layers can be written as^{61,62}

$$\mathcal{H}_0(\mathbf{k}) = \begin{pmatrix} \epsilon_0(\mathbf{k}) + \mathbf{h}_A(\mathbf{k}) \cdot \boldsymbol{\sigma} & V_{AB}(\mathbf{k}) \\ V_{AB}(\mathbf{k}) & \epsilon_0(\mathbf{k}) + \mathbf{h}_B(\mathbf{k}) \cdot \boldsymbol{\sigma} \end{pmatrix}. \quad (38)$$

Here, $\epsilon_0(\mathbf{k}) = -t(\cos k_x + \cos k_y)$ and $V_{AB}(\mathbf{k}) = -2\tilde{t} \cos(k_x/2) \cos(k_y/2)$ describes the hopping between the same and different sublattices, with $t = 0.08$ eV and $\tilde{t} = 1$ eV being the respective hopping amplitudes. The anisotropic SOC and exchange energy enter in the second term in the diagonal blocks $\mathbf{h}_A(\mathbf{k}) = -\mathbf{h}_B(\mathbf{k}) = \{h_{\text{AF}}^x - \alpha_R \sin k_y, h_{\text{AF}}^y + \alpha_R \sin k_x, h_{\text{AF}}^z\}$, where $\alpha_R = 0.8$ eV is the SOC parameter. The Néel vector lies in the xy plane, making an angle ϕ with the x axis, $\hat{\mathbf{n}} = (\cos \phi, \sin \phi, 0)$. Accordingly, we write the exchange field as $\mathbf{h}_{\text{AF}} = \{h_{\text{AF}}^x, h_{\text{AF}}^y, h_{\text{AF}}^z\} = J_n \hat{\mathbf{n}}$, with $J_n = 0.85$ eV⁶². The energy eigenvalues of the above Hamiltonian are

$$\varepsilon_{\pm}(\mathbf{k}) = \epsilon_0(\mathbf{k}) \pm \sqrt{|\mathbf{h}_A(\mathbf{k})|^2 + V_{AB}(\mathbf{k})^2}, \quad (39)$$

where \pm correspond to the doubly degenerate conduction and valence bands, respectively. The resulting band gap,

$$\delta\varepsilon(\mathbf{k}) = 2\sqrt{|\mathbf{h}_A(\mathbf{k})|^2 + V_{AB}^2(\mathbf{k})}, \quad (40)$$

is tunable through the orientation of the Néel vector. We present the band structure of CuMnAs in Fig. 2(b) for three different orientations of Néel vector.

Since the system preserves \mathcal{PT} symmetry, $\chi_{a;d}^{\text{IG,CMV}}$ is symmetry-forbidden, leaving the magnetic field-induced charge polarization oscillation as the sole source of IGMC. The momentum-space distributions of the underlying band geometric quantities, *spin*-MBCP and *orbital*-MBCP, are displayed in Figs. 2(c) and 2(d). The color scale of the plots indicates that the *orbital*-MBCP contribution is almost an order of magnitude larger than the *spin*-MBCP contribution.

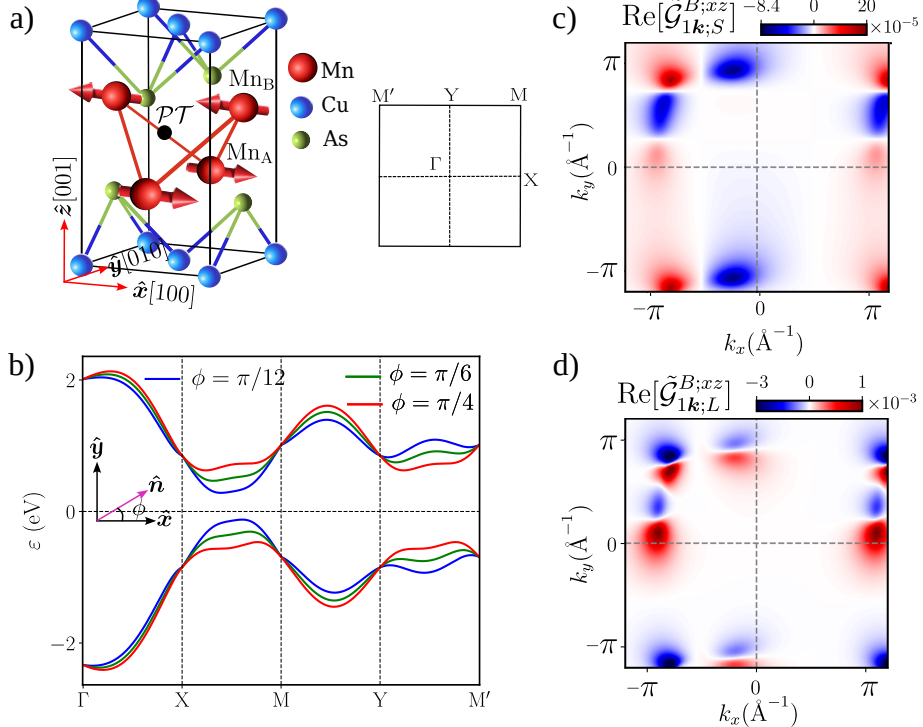


FIG. 2. (a) Crystallographic and magnetic structure of tetragonal CuMnAs. The red arrows indicate the direction of magnetic moments. The projected Brillouin zone in the $x-y$ plane, along with high-symmetry points, is also shown. (b) The band dispersion for three different orientations of the Néel vector, $\phi = \{\pi/12, \pi/6, \pi/4\}$. Here, ϕ is the angle made by the Néel vector (\hat{n}) with \hat{x} ([100]) axis. (c), (d) The momentum space distribution of *spin*-MBCP ($\tilde{G}_{1k;S}^{B;xz}$) and *orbital*-MBCP ($\tilde{G}_{1k;L}^{B;xz}$) for the first conduction band for Néel angle $\phi = \pi/4$.

For a magnetic field along the \hat{z} axis of the crystal, the IGMC tensors $\chi_{x;z}^{\text{IGMC}}$ and $\chi_{y;z}^{\text{IGMC}}$ are restricted by the microscopic symmetry of the material. In tetragonal CuMnAs, the crystalline symmetry can be controlled by the Néel vector orientation. When the Néel vector aligns along \hat{x} , the system posses \mathcal{M}_x symmetry but breaks \mathcal{M}_y . Consequently, the system allows only $\chi_{x;z}^{\text{IGMC}}$ response but prohibits $\chi_{y;z}^{\text{IGMC}}$ (See Table III). Rotating the Néel vector to \hat{y} reverses the symmetry configuration: \mathcal{M}_x is lost and \mathcal{M}_y is preserved. This suppresses $\chi_{x;z}^{\text{IGMC}}$, but allows $\chi_{y;z}^{\text{IGMC}}$. A continuous rotation of the Néel vector between these two high-symmetry directions induces a smooth transfer of mirror symmetry, and the IGMC evolves accordingly: $\chi_{x;z}^{\text{IGMC}}$ decreases while $\chi_{y;z}^{\text{IGMC}}$ increases. This is in agreement with Figs. 3(a) and 3(b). The variation in the IGMC amplitude can also be attributed to the evolution of the *spin*- and *orbital*-MBCP tensors. A rotation of the Néel vector modifies the band gap, and because the MBCP tensors scale inversely with band gap, their magnitudes and the associated IGMC tensors change accordingly. From Fig. 3(c), we note that for a fixed Néel orientation, $\chi_{x;z}^{\text{IGMC}}(\omega)$ remains constant when the chemical potential lies within the band gap. This is due to the Fermi sea nature of IGMC.

Notably, the IGMC conductivity in \mathcal{PT} -symmetric ma-

terials is a \mathcal{T} -odd response, and its sign reverses when the magnetization order, or the Néel vector, switches direction. This can be seen from Figs. 3(b). This symmetry-protected sign change makes IGMC a sensitive probe of the Néel vector orientation in CuMnAs and, more broadly, in other \mathcal{PT} -symmetric antiferromagnets.

We compare the *spin*-MBCP and *orbital*-MBCP contributions in Fig. 3(d). Even though CuMnAs has a finite SOC, the spin contribution to IGMC arising from the $\tilde{G}_{n;S}^{B;ad}$ is almost an order (~ 20 times) of magnitude smaller than its orbital counterpart stemming from $\tilde{G}_{n;L}^{B;ad}$. This highlights the significance of the orbital contribution for IGMC responses even in SOC materials.

To demonstrate the experimental feasibility of predicted results, we estimate the electric voltage arising from IGMC. We use the results from the 2D model for CuMnAs layers and convert the computed gyrotropic conductivity into an effective 3D conductivity by dividing it by interlayer spacing, $c = 6.32$ Å for CuMnAs⁶³. The electrical voltage is given by $V = \chi_{x;z}^{3D} B_0 \rho l$, with ρ and l are being the longitudinal resistivity and length of the sample, respectively and $\chi_{x;z}^{3D} = (\chi_{x;z}^{\text{IGMC}}/c)$. By taking a representative values of $\rho = 50 \mu\Omega \text{ cm}$ ⁶⁴, $l = 100 \mu\text{m}$ and the maximum value of $\chi_{x;z}^{\text{IGMC}}$ from Fig. (3a), the electric voltage is estimated to be $V = 0.2 \text{ mV}$ for a magnetic

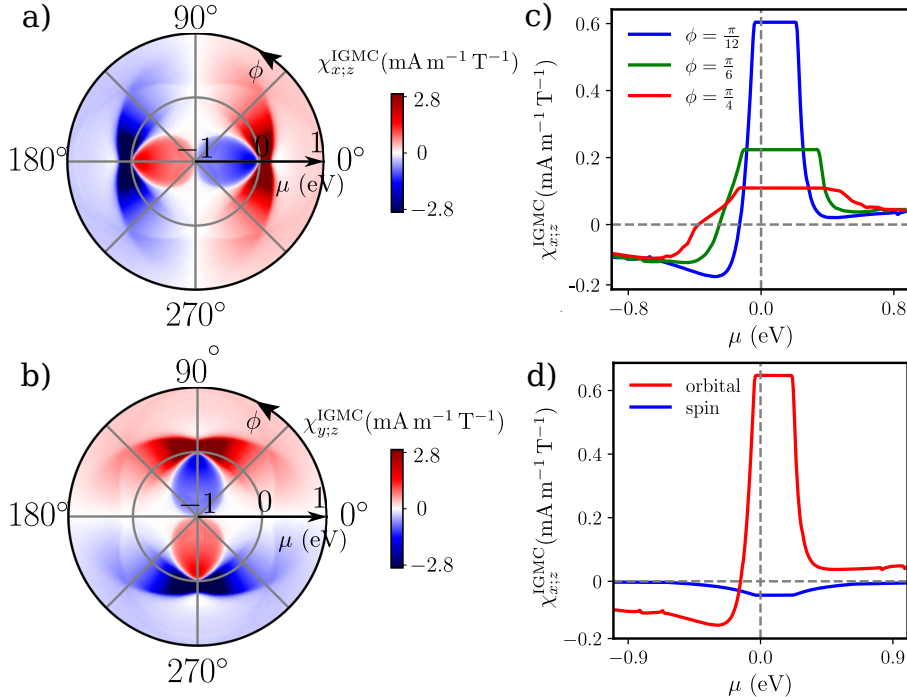


FIG. 3. (a), (b): Intrinsic gyrotropic magnetic conductivities $\chi_{x;z}^{\text{IGMC}}$ and $\chi_{y;z}^{\text{IGMC}}$ as functions of the Néel vector angle ϕ and chemical potential μ . The polar angle ϕ is measured from the \hat{x} axis, parallel to the crystallographic [100] direction. (c) Chemical potential dependence of $\chi_{x;z}^{\text{IGMC}}$ for three representative Néel orientations. (d) *orbital*- and *Spin*-MBCP contributions to $\chi_{x;z}^{\text{IGMC}}$ at $\phi = \pi/12$. For all plots, the magnetic driving frequency is assumed to be $\hbar\omega = 1 \mu\text{eV}$. The orbital response dominates the spin contribution by almost an order of magnitude. The IGMC response in the band gap highlights that it is a Fermi sea response, and it measures the total ‘magnetic polarizability’ of all the filled bands.

field strength $B_0 = 1 \text{ T}$. This is well within experimental reach.

VI. CONCLUSION

To summarize, we have developed a microscopic theory of the gyrotropic magnetic current that unifies the orbital mechanism with the recently proposed spin-driven magnetic displacement contribution. Crucially, we identify the orbital component of the magnetic displacement current, which has not been explored earlier.

Starting from a magnetic quantum kinetic equation with both spin-Zeeman and orbital coupling, we derived the finite-frequency semiclassical Lagrangian and the corresponding equations of motion. This naturally yields a magnetic field induced Berry connection correction, with both spin and orbital contributions. The orbital contribution includes an additional term that was overlooked in earlier semiclassical treatments. To quantify these effects, we introduce two band-geometric quantities: the spin and orbital magnetic Berry connection polarizabilities. When integrated over the Brillouin zone, the Berry-connection correction generates a magnetic field induced charge polarization. The temporal modulation of the charge polarization produces the magnetic displacement

current. This displacement current can also have an intrinsic contribution, giving rise to IGMC.

Our symmetry analysis reveals that this intrinsic gyrotropic magnetic current is finite in inversion-broken systems that preserve combined inversion and time-reversal symmetry, where the conventional gyrotropic conductivity vanishes. Guided by the symmetry analysis, we demonstrate the effect in tetragonal CuMnAs. We find that the orbital contribution dominates over the spin channel by nearly an order of magnitude, establishing the orbital mechanism as the leading source of IGMC. Moreover, the IGMC response is tunable by the Néel vector orientation and, being time-reversal-odd, it reverses sign upon Néel vector reversal. This Néel vector dependent sign change identifies IGMC as a direct and experimentally accessible probe of antiferromagnetic order in CuMnAs and related bipartite antiferromagnets.

VII. ACKNOWLEDGMENT

We thank Sunit Das (IIT Kanpur, India) for many fruitful discussions. K.G. acknowledges the Ministry of Education, Government of India, for financial support through the Prime Minister’s Research Fellowship. S.S. is supported by the Indian Institute of Technology Kan-

pur. A.A. acknowledges funding from the Core Research Grant by ANRF (Sanction No. CRG/2023/007003), Department of Science and Technology, India.

Appendix A: Density matrix calculation in the presence of an oscillating magnetic field

In this section, we study the dynamics of Bloch electrons in the presence of an oscillating magnetic field. In the absence of any external field, the distribution of Bloch electrons is characterized by the equilibrium Fermi-Dirac distribution function: $f_n = [1 + e^{\beta(\varepsilon_{n\mathbf{k}} - \mu)}]^{-1}$, where $\varepsilon_{n\mathbf{k}}$ is the n^{th} band energy eigenvalue, μ is the chemical potential, $\beta = 1/(k_B T)$ with k_B is Boltzmann constant and T is absolute temperature of the system. The external magnetic field drives the system into a nonequilibrium state, which gives rise to the response in experimental measurements. To describe this nonequilibrium state and to account for the effects of the external magnetic field, we use the nonequilibrium density matrix of the Bloch electrons, which is obtained by solving the quantum Liouville equation. In our study, we consider an oscillating magnetic field of frequency ω , defined as:

$$\mathbf{B}(t) = \frac{1}{2} \mathbf{B}_0 (e^{i\omega t} + e^{-i\omega t}) . \quad (\text{A1})$$

This magnetic field interacts with an electron's magnetic moment in two different ways: (i) minimal coupling with orbital degree of freedom, and (ii) Zeeman coupling with spin degree of freedom. Considering these two types of couplings, the total magnetic interaction can be expressed as

$$\hat{\mathcal{H}}^B = \hat{\mathcal{H}}_L^B + \hat{\mathcal{H}}_S^B = -\mathbf{B} \cdot \hat{\mathcal{M}}^L - \mathbf{B} \cdot \hat{\mathcal{M}}^S , \quad (\text{A2})$$

where, $\hat{\mathcal{M}}^L = -(e/4)[\hat{\mathbf{r}} \times \hat{\mathbf{v}} - \hat{\mathbf{v}} \times \hat{\mathbf{r}}]$ is the orbital magnetic momentum operator, and $\hat{\mathcal{M}}^S = -(g_s \mu_B/2)\hat{\boldsymbol{\sigma}}$ is the spin magnetic moment operator. Here, g_s is the spin g -factor, μ_B is the Bohr magneton, and $\hat{\boldsymbol{\sigma}} = (\hat{\sigma}_x, \hat{\sigma}_y, \hat{\sigma}_z)$ corresponds to the Pauli spin matrices. In the presence of this magnetic field, the quantum Liouville equation can be written in the form³⁸:

$$\frac{\partial \hat{\rho}}{\partial t} + \frac{i}{\hbar} [\hat{\mathcal{H}}_0, \hat{\rho}] + \frac{1}{\tau} \hat{\rho} = \mathcal{D}_B \hat{\rho} - \frac{i g_s \mu_B}{2\hbar} \mathbf{B} \cdot [\hat{\boldsymbol{\sigma}}, \hat{\rho}] . \quad (\text{A3})$$

Here, $\hat{\mathcal{H}}_0$ denotes the unperturbed Bloch Hamiltonian, which satisfies $\hat{\mathcal{H}}_0 |u_{n\mathbf{k}}\rangle = \varepsilon_{n\mathbf{k}} |u_{n\mathbf{k}}\rangle$, with $|u_{n\mathbf{k}}\rangle$ being the cell-periodic part of the Bloch state. In Eq. (A3), τ is a phenomenological scattering time that characterizes the relaxation of the perturbed system. The first term on the right-hand side of Eq. (A3), $\mathcal{D}_B \hat{\rho}$, captures the interaction between the magnetic field and orbital moment. The matrix elements of this term, in the Bloch basis, are given by

$$[\mathcal{D}_B \hat{\rho}]_{nm} = \frac{e}{2\hbar^2} \{(\mathcal{D}_{\mathbf{k}} \hat{\mathcal{H}}_0 \times \mathbf{B}) \cdot \mathcal{D}_{\mathbf{k}} \hat{\rho}\}_{nm} = \frac{e}{2\hbar^2} B^c \epsilon_{cab} \{\mathcal{D}_b \hat{\mathcal{H}}_0, \mathcal{D}_a \hat{\rho}\}_{nm} . \quad (\text{A4})$$

In Eq. (A4), the notation $\{\mathbf{p} \cdot \mathbf{q}\} = \mathbf{p} \cdot \mathbf{q} + \mathbf{q} \cdot \mathbf{p}$ (with \mathbf{p} and \mathbf{q} being vector operators) denotes a symmetrized operator product and $\mathcal{D}_a \hat{\mathcal{X}} \equiv \mathcal{D} \hat{\mathcal{X}} / \mathcal{D} k_a$, where the action of covariant derivative $\mathcal{D}_{\mathbf{k}} \equiv \mathcal{D} / \mathcal{D} \mathbf{k}$ on a matrix operator $\hat{\mathcal{X}}$ is defined as follows:

$$[\mathcal{D}_{\mathbf{k}} \hat{\mathcal{X}}]_{nm} \equiv \left(\frac{\mathcal{D} \hat{\mathcal{X}}}{\mathcal{D} \mathbf{k}} \right)_{nm} = \partial_{\mathbf{k}} \mathcal{X}_{nm} - i [\hat{\mathcal{R}}, \hat{\mathcal{X}}]_{nm} . \quad (\text{A5})$$

In the above equation, $\partial_{\mathbf{k}} \equiv \partial / \partial \mathbf{k}$ -denotes simple derivative with respect to crystal momentum and $[\hat{\mathcal{R}}]_{nm} \equiv \mathcal{R}_{nm} = \langle u_{n\mathbf{k}} | i \partial_{\mathbf{k}} | u_{m\mathbf{k}} \rangle$ is the band-resolved Berry connection.

In the weak field limit, we can treat the magnetic interaction as a perturbation over the crystal Hamiltonian. In this situation, Eq. (A3) is solved perturbatively to obtain density matrix elements at different orders in magnetic field strength. The N^{th} order correction to the density matrix, $\hat{\rho}^{(B^N)} (\sim |\mathbf{B}|^N)$ can be expressed as,

$$(\partial_t + \mathcal{E}) \hat{\rho}^{(B^N)} = \mathcal{D}_B \hat{\rho}^{(B^{N-1})} - \frac{i g_s \mu_B}{2\hbar} \mathbf{B} \cdot [\hat{\boldsymbol{\sigma}}, \hat{\rho}^{(B^{N-1})}] , \quad (\text{A6})$$

where we have defined $\mathcal{E} = (\mathcal{P} + 1/\tau)$ with $\mathcal{P} \hat{\rho} = (i/\hbar)[\hat{\mathcal{H}}_0, \hat{\rho}]$ for compactness of the equation.

Solution for first order density matrix equation

The intrinsic gyrotropic magnetic current depends on the first-order density matrix elements. Inserting $N = 1$ into Eq. (A6), we get the quantum Liouville equation for first order density matrix, $\hat{\rho}^B$, as follows:

$$\frac{\partial \hat{\rho}^B}{\partial t} + \frac{i}{\hbar} [\hat{\mathcal{H}}_0, \hat{\rho}^B] + \frac{1}{\tau} \hat{\rho}^B = \mathcal{D}_B \hat{\rho}^{(0)} - \frac{i g_s \mu_B}{2\hbar} \mathbf{B} \cdot [\hat{\boldsymbol{\sigma}}, \hat{\rho}^{(0)}]. \quad (\text{A7})$$

Here, $\hat{\rho}^{(0)}$ denotes the density matrix of the Bloch electrons in the absence of a magnetic field, given by $\rho_{nm}^{(0)} = \delta_{nm} f_n$. In the steady state, the time dependence of the density matrix could only be carried in its' dynamic phase

$$\rho_{nm}^B(t) = \rho_{nm}^B(\omega) e^{i\omega t} + \rho_{nm}^B(-\omega) e^{-i\omega t}. \quad (\text{A8})$$

We substitute this *ansatz* into Eq. (A7) to obtain the off-diagonal elements of the first-order density matrix, which are

$$\begin{aligned} \rho_{nm}^B(\omega) &= \frac{1}{\frac{1}{\tau} + i(\omega_{nm} + \omega)} \frac{e}{4\hbar^2} \{(\mathcal{D}_B \hat{\mathcal{H}}_0 \times \mathbf{B}_0) \cdot \mathcal{D}_B \hat{\rho}^{(0)}\}_{nm} - \frac{1}{\frac{1}{\tau} + i(\omega_{nm} + \omega)} \frac{i g_s \mu_B}{4\hbar} \mathbf{B}_0 \cdot [\hat{\boldsymbol{\sigma}}, \hat{\rho}^{(0)}]_{nm} \\ &= \frac{e}{4\hbar^2} g_{nm}^\omega \epsilon_{cab} B_0^c \{ \mathcal{D}_b \hat{\mathcal{H}}_0, \mathcal{D}_a \hat{\rho}^{(0)} \}_{nm} + \frac{i g_s \mu_B}{4\hbar} g_{nm}^\omega (\mathbf{B}_0 \cdot \boldsymbol{\sigma}_{nm}) f_{nm} \\ &= \rho_{nm;L}^B(\omega) + \rho_{nm;S}^B(\omega), \end{aligned} \quad (\text{A9})$$

where $g_{nm}^\omega = [1/\tau + i(\omega_{nm} + \omega)]^{-1}$ and $f_{nm} = f_n - f_m$. The matrix elements of the covariant derivative of \mathcal{H}_0 and $\hat{\rho}^{(0)}$ are given by

$$[\mathcal{D}_b \hat{\mathcal{H}}_0]_{nm} = \hbar [\delta_{nm} v_n^b + i\omega_{nm} \mathcal{R}_{nm}^b] = \hbar [\delta_{nm} v_n^b + v_{nm}^b], \quad (\text{A10})$$

$$[\mathcal{D}_a \hat{\rho}_0]_{nm} = [\delta_{nm} (\partial_a f_n) + i f_{nm} \mathcal{R}_{nm}^a], \quad (\text{A11})$$

where, $v_{nm}^b = i\omega_{nm} \mathcal{R}_{nm}^b$ is the off-diagonal velocity matrix element. The first part of Eq. (A9), $\rho_{nm;L}^B(\omega)$, corresponds to the orbital contribution to the off-diagonal density matrix and the second part, $\rho_{nm;S}^B(\omega)$, depicts the spin contribution. Notably, the spin part depends on the off-diagonal spin matrix element. Therefore, this contribution depends on the spin-orbit coupling (SOC) strength of the material and would be negligible in materials with low SOC. While the orbital part is not restricted to any such condition, it would be prevalent in all materials. Substitution of the covariant derivatives from Eqs. (A10) and (A11) into the orbital part yields

$$\begin{aligned} \rho_{nm;L}^B(\omega) &= \frac{e}{4\hbar^2} g_{nm}^\omega \epsilon_{cab} B_0^c \left\{ \mathcal{D}_b \hat{\mathcal{H}}_0, \mathcal{D}_a \hat{\rho}^{(0)} \right\}_{nm} \\ &= \frac{e}{4\hbar^2} g_{nm}^\omega \epsilon_{cab} B_0^c \sum_p \left([\mathcal{D}_b \hat{\mathcal{H}}_0]_{np} [\mathcal{D}_a \hat{\rho}^{(0)}]_{pm} + [\mathcal{D}_a \hat{\rho}^{(0)}]_{np} [\mathcal{D}_b \hat{\mathcal{H}}_0]_{pm} \right) \\ &= \frac{e}{4\hbar^2} g_{nm}^\omega \epsilon_{cab} B_0^c \sum_p \left(\hbar [\delta_{np} v_n^b + v_{np}^b] [\delta_{pm} (\partial_a f_m) + i f_{pm} \mathcal{R}_{pm}^a] + [\delta_{np} (\partial_a f_n) + i f_{np} \mathcal{R}_{np}^a] \hbar [\delta_{pm} v_m^b + v_{pm}^b] \right) \\ &= \frac{e}{4\hbar} g_{nm}^\omega \mathbf{B}_0 \cdot [\partial_{\mathbf{k}} (f_n + f_m) \times \mathbf{v}_{nm}] - \frac{ie}{4\hbar} g_{nm}^\omega \mathbf{B}_0 \cdot \sum_{p \neq m} (\mathbf{v}_{np} + \delta_{np} \mathbf{v}_m) \times \mathbf{R}_{pm} f_{pm} \\ &\quad + \frac{ie}{4\hbar} g_{nm}^\omega \mathbf{B}_0 \cdot \sum_{p \neq n} \mathbf{R}_{np} \times (\mathbf{v}_{pm} + \delta_{pm} \mathbf{v}_n) f_{np}. \end{aligned} \quad (\text{A12})$$

From Eq. (A9), the spin part of the off-diagonal density matrix is given by

$$\rho_{nm;S}^B(\omega) = \frac{i g_s \mu_B}{4\hbar} g_{nm}^\omega (\mathbf{B}_0 \cdot \boldsymbol{\sigma}_{nm}) f_{nm}. \quad (\text{A13})$$

Appendix B: Derivation of semiclassical Lagrangian from density matrix framework

The semiclassical transport theory presents a simplified understanding of intraband dynamics of charge carriers under small perturbations. While the density matrix framework extends the understanding by including the interband

dynamics. The motivation of this section is to unify these two different pictures by deriving the equation of motion (EOM) from the density matrix formalism in the semiclassical limit. Semiclassical description is valid only in the regime where (i) the spatial variations of the external fields are slow over the wavepacket extension, and (ii) the temporal variation doesn't induce any real interband transition. We respect the first criterion by assuming a standard semiclassical perturbation in the density matrix picture, and maintain the second by reducing terms into an effective single-band form. The basic recipes that we follow are: (i) to derive the Lagrangian using density matrix formalism and reduce it into a single-band expression, and then (ii) use the Euler-Lagrangian equations to derive the EOM. The Lagrangian operator for a system can be defined as follows:

$$\hat{\mathcal{L}} = i\hbar \frac{\partial}{\partial t} - \hat{\mathcal{H}} . \quad (\text{B1})$$

In the density matrix picture, the Lagrangian of the system can be calculated following a trace of the combined Lagrangian and density matrix operator over the Bloch states:

$$\begin{aligned} \mathcal{L}_k &= \text{Tr}\{\hat{\mathcal{L}}\hat{\rho}\} \\ &= \sum_n \langle u_{nk} | \left(i\hbar \frac{\partial}{\partial t} - \hat{\mathcal{H}} \right) \hat{\rho} | u_{nk} \rangle \\ &= \sum_n \langle u_{nk} | \left(i\hbar \frac{\partial \hat{\rho}}{\partial t} + i\hbar \hat{\rho} \frac{\partial}{\partial t} - \hat{\mathcal{H}} \hat{\rho} \right) | u_{nk} \rangle \\ &= i\hbar \sum_n \langle u_{nk} | \frac{\partial \hat{\rho}}{\partial t} | u_{nk} \rangle + i\hbar \sum_n \langle u_{nk} | \hat{\rho} \left| \frac{\partial u_{nk}}{\partial t} \right\rangle - \sum_n \langle u_{nk} | \hat{\mathcal{H}} \hat{\rho} | u_{nk} \rangle \\ &= i\hbar \sum_n \frac{\partial \rho_{nn}}{\partial t} + i\hbar \sum_{np} \langle u_{nk} | \hat{\rho} | u_{pk} \rangle \left\langle u_{pk} \left| \frac{\partial u_{nk}}{\partial t} \right. \right\rangle - \sum_n \langle u_{nk} | \hat{\mathcal{H}} \hat{\rho} | u_{nk} \rangle \\ &= i\hbar \sum_n \frac{d\rho_{nn}}{dt} - i\hbar \sum_n \dot{\mathbf{k}} \cdot \frac{\partial \rho_{nn}}{\partial \mathbf{k}} + i\hbar \sum_{np} \rho_{np} \left\langle u_{pk} \left| \frac{\partial u_{nk}}{\partial t} \right. \right\rangle - \sum_n \langle u_{nk} | \hat{\mathcal{H}} \hat{\rho} | u_{nk} \rangle \\ &= -i\hbar \sum_n \dot{\mathbf{k}} \cdot \frac{\partial \rho_{nn}}{\partial \mathbf{k}} + i\hbar \sum_{np} \rho_{np} \left\langle u_{pk} \left| \frac{\partial u_{nk}}{\partial t} \right. \right\rangle - \sum_n \langle u_{nk} | \hat{\mathcal{H}} \hat{\rho} | u_{nk} \rangle . \end{aligned} \quad (\text{B2})$$

In the above expression, we have dropped the unnecessary total time derivative of the nonequilibrium density matrix ρ_{nn} , since that would not affect the result of the Euler-Lagrangian equations. The first term involving the crystal momentum derivative of the density matrix can be expressed in terms of the position operator expectation value. The average electronic position \mathbf{r} within an unit cell can be defined as follows,

$$\begin{aligned} \mathbf{r} = \langle \hat{\mathbf{r}} \rangle = \text{Tr}\{\hat{\mathbf{r}}\hat{\rho}\} &= \sum_{np} \mathbf{r}_{np} \rho_{pn} = \sum_{np} (i\delta_{np} \partial_{\mathbf{k}} + \mathbf{R}_{np}) \rho_{pn} , \\ \Rightarrow \sum_n \mathbf{r}_n \rho_{nn} &= \sum_n \left[i \frac{\partial \rho_{nn}}{\partial \mathbf{k}} + \sum_p \rho_{np} \mathbf{R}_{pn} \right] \\ \Rightarrow i \frac{\partial \rho_{nn}}{\partial \mathbf{k}} &= \mathbf{r}_n \rho_{nn} - \sum_p \rho_{np} \mathbf{R}_{pn} , \end{aligned} \quad (\text{B3})$$

where we have defined $\mathbf{r} = \sum_n \mathbf{r}_n \rho_{nn}$ with \mathbf{r}_n being the effective single band expression of \mathbf{r} . Substituting the result from Eq. (B3) into Eq. (B2) leads to the final expression of Lagrangian,

$$\mathcal{L}_k = - \sum_n \hbar \dot{\mathbf{k}} \cdot \left(\mathbf{r}_n \rho_{nn} - \sum_p \rho_{np} \mathbf{R}_{pn} \right) + i\hbar \sum_{np} \rho_{np} \left\langle u_{pk} \left| \frac{\partial u_{nk}}{\partial t} \right. \right\rangle - \sum_n \langle u_{nk} | \hat{\mathcal{H}} \hat{\rho} | u_{nk} \rangle . \quad (\text{B4})$$

The Bloch states in the presence of a magnetic field take the form $e^{i\mathbf{k} \cdot \mathbf{r}} |u_n(\mathbf{k} + e\mathbf{A}(\mathbf{r})/\hbar)\rangle$, where $\mathbf{A} = \frac{1}{2}(\mathbf{B} \times \mathbf{r})$ is the magnetic vector potential in symmetric gauge. In the presence of a magnetic field, \mathbf{k} becomes gauge-dependent, and thereby we replace \mathbf{k} in Eq. (B4) with the gauge-invariant crystal momentum $\mathbf{\kappa} = \mathbf{k} + (e/\hbar)\mathbf{A}(\mathbf{r})$. Here, we denote the charge of an electron by $-e$, with $e > 0$.

Now, we evaluate each of the three terms in Eq. (B4) separately. For the first term, we replace \mathbf{k} with $\mathbf{\kappa}$ and use Eq. (B3) to obtain

$$\sum_n \hbar \dot{\mathbf{k}} \cdot \left(-i \frac{\partial \rho_{nn}}{\partial \mathbf{k}} \right) = - \sum_n \left[\hbar \dot{\mathbf{k}} - \frac{e}{2} \mathbf{B}(t) \times \dot{\mathbf{r}}_n \right] \cdot \left[\mathbf{r}_n \rho_{nn} - \sum_p \rho_{np} \mathcal{R}_{pn} \right]. \quad (\text{B5})$$

We calculate the second term in Eq. (B4) using the completeness of the Bloch basis and the partial time derivative of the Bloch state:

$$\begin{aligned} i\hbar \sum_{np} \rho_{np} \left\langle u_{p\kappa} \left| \frac{\partial u_{n\kappa}}{\partial t} \right. \right\rangle &= i \sum_n \rho_{np} \left(\hbar \frac{\partial \kappa}{\partial t} \right) \cdot \left\langle u_{p\kappa} \left| \frac{\partial u_{n\kappa}}{\partial \kappa} \right. \right\rangle \\ &= \frac{e}{2} (\mathbf{B} \times \dot{\mathbf{r}}_n) \cdot \sum_p \rho_{np} \mathcal{R}_{pn}. \end{aligned} \quad (\text{B6})$$

The third term of Eq. (B4) corresponds to the magnetic field induced total energy:

$$\sum_n \langle u_{n\kappa} | \hat{\mathcal{H}} \hat{\rho} | u_{n\kappa} \rangle = \sum_n \tilde{\varepsilon}_{n\kappa} \rho_{nn}. \quad (\text{B7})$$

Here, $\tilde{\varepsilon}_{n\kappa}$ denotes the field-corrected band energy. Substituting the results from Eqs. (B5), (B6) and (B7) into Eq. (B4) yields the total Lagrangian,

$$\mathcal{L}_\kappa = - \sum_n \hbar \dot{\mathbf{k}} \cdot \left[\mathbf{r}_n \rho_{nn} - \left(\rho_{nn} \mathcal{R}_{n\kappa} + \sum_{p \neq n} \rho_{np}(t) \mathcal{R}_{pn} \right) \right] + \frac{e}{2} \sum_n [\mathbf{B}(t) \times \dot{\mathbf{r}}_n] \cdot \mathbf{r}_n \rho_{nn} - \sum_n \tilde{\varepsilon}_{n\kappa} \rho_{nn}. \quad (\text{B8})$$

To extract the band-resolved Lagrangian from the total Lagrangian, we need to recast the second term inside the parentheses as an effective single-band quantity. Interestingly, this term yields a magnetic field induced Berry connection, as derived in Eq. (B28). Using the expression from Eq. (B28), the total Lagrangian can be written as

$$\mathcal{L}_\kappa = - \sum_n \hbar \dot{\mathbf{k}} \cdot \left[\mathbf{r}_n \rho_{nn} - \left(\mathcal{R}_{n\kappa} \rho_{nn} + \mathcal{R}_{n\kappa}^B(t) f_n \right) \right] + \frac{e}{2} \sum_n [\mathbf{B}(t) \times \dot{\mathbf{r}}_n] \cdot \mathbf{r}_n \rho_{nn} - \sum_n \tilde{\varepsilon}_{n\kappa} \rho_{nn}. \quad (\text{B9})$$

For simplicity, from now onwards, we represent the gauge-invariant crystal momentum κ by \mathbf{k} . Recently, the unification^{21,65} of quantum kinetic framework and semiclassical transport theory for electric driving has been demonstrated from the perspective of charge current: $\mathbf{J} = \text{Tr}(\hat{\mathbf{v}} \hat{\rho}) = \sum_n (\hat{\mathbf{v}} \hat{\rho})_{nn} = \sum_n \dot{\mathbf{r}}_n g_n$, where $\dot{\mathbf{r}}_n$ is the wavepacket velocity and g_n corresponds to the nonequilibrium Boltzmann distribution function. Similarly, if the semiclassical band-momentum resolved Lagrangian be $\mathcal{L}_{n\kappa}^S$, momentum resolved total Lagrangian in presence of a magnetic field would be $\mathcal{L}_\kappa = \sum_n \mathcal{L}_{n\kappa}^S D_{n\kappa}^{-1} f_{n\kappa}$, where $D_{n\kappa}^{-1} = [1 + e/\hbar(\mathbf{B} \cdot \Omega_{n\kappa})]$ is the magnetic field corrected phase factor. The magnetic field induced diagonal density matrix can be calculated to be $\rho_{nn} = [1 + e/\hbar(\mathbf{B} \cdot \Omega_{n\kappa})] f_{n\kappa} = D_{n\kappa}^{-1} f_{n\kappa}$ ³⁸. Thereby, the correct quantity to compare with $\mathcal{L}_{n\kappa}^S$ would be $\mathcal{L}_{n\kappa}$, defined in the following way,

$$\mathcal{L}_\kappa = \sum_n \mathcal{L}_{n\kappa} \rho_{nn}. \quad (\text{B10})$$

Now, comparing Eqs. (B9) and (B10), and collecting terms up to second order in the magnetic field strength, we obtain the band-resolved Lagrangian to be

$$\mathcal{L}_{n\kappa} = - \hbar \dot{\mathbf{k}} \cdot \left[\mathbf{r}_n - \left(\mathcal{R}_{n\kappa} + \mathcal{R}_{n\kappa}^B(t) \right) \right] + \frac{e}{2} [\mathbf{B}(t) \times \dot{\mathbf{r}}_n] \cdot \mathbf{r}_n - \tilde{\varepsilon}_{n\kappa}. \quad (\text{B11})$$

To our knowledge, this is the first work to capture the effect of the time dependence of a magnetic field via minimal coupling interaction. In the dc limit, this result matches the existing semiclassical theory^{19,45}, except that we obtain an extra term in the magnetic field induced Berry connection. The expression of the *a.c* magnetic field corrected Berry connection, along with its zero-frequency result, is derived below.

Magnetic field induced Berry connection correction

Here, we aim to derive the density matrix formulation of the magnetic field induced Berry connection correction. For this, we plug in the magnetic field induced off-diagonal density matrix elements from Eq. (A9) into $\sum_{n,m \neq n} \rho_{nm} \mathcal{R}_{mn}^a$,

and express the resultant expression into an effective single band term. Because the density matrix accounts for both minimal coupling and Zeeman interaction, the resulting Berry connection correction contains contributions from both orbital and spin magnetic moments,

$$\sum_{n,m \neq n} \rho_{nm}^B(t) \mathcal{R}_{mn}^a = \left[\sum_{n,m \neq n} \rho_{nm;L}^B(\omega) \mathcal{R}_{mn}^a e^{i\omega t} + \sum_{n,m \neq n} \rho_{nm;S}^B(\omega) \mathcal{R}_{mn}^a e^{i\omega t} \right] + (\omega \rightarrow -\omega) . \quad (\text{B12})$$

As shown below, the first term in Eq. (B12) gives rise to the orbital contribution, while the second term yields the spin contribution to the Berry connection correction. For convenience, we calculate these two contributions separately.

a. Orbital part of the Berry connection correction

The orbital part of the magnetic field driven Berry connection correction can be obtained by evaluating the term

$$\sum_{n,m \neq n} \rho_{nm;L}^B(t) \mathcal{R}_{mn}^a = \sum_{n,m \neq n} \rho_{nm;L}^B(\omega) \mathcal{R}_{mn}^a e^{i\omega t} + (\omega \rightarrow -\omega) . \quad (\text{B13})$$

Here, we have

$$\begin{aligned} \sum_{n,m \neq n} \rho_{nm;L}^B(\omega) \mathcal{R}_{mn}^a e^{i\omega t} &= e^{i\omega t} \frac{e}{4\hbar} \sum_{n,m \neq n} g_{nm}^\omega \mathbf{B}_0 \cdot [\{\partial_{\mathbf{k}}(f_n + f_m)\} \times \mathbf{v}_{nm}] \mathcal{R}_{mn}^a \\ &\quad - e^{i\omega t} \frac{ie}{4\hbar} \sum_{n,m \neq n} g_{nm}^\omega \mathbf{B}_0 \cdot \sum_{p \neq m} [(\mathbf{v}_{np} + \delta_{np} \mathbf{v}_m) \times \mathcal{R}_{pm}] \mathcal{R}_{mn}^a f_{pm} \\ &\quad + e^{i\omega t} \frac{ie}{4\hbar} \sum_{n,m \neq n} g_{nm}^\omega \mathbf{B}_0 \cdot \sum_{p \neq n} [\mathcal{R}_{np} \times (\mathbf{v}_{pm} + \delta_{pm} \mathbf{v}_n)] \mathcal{R}_{mn}^a f_{np} . \end{aligned} \quad (\text{B14})$$

Following the invariance of dummy indices, we exchange $m \leftrightarrow n$ in the first term. For the second and third terms, we unpack the population difference and exchange indices $p \leftrightarrow n$ into the terms associated with f_p , thereby recasting the entire expression as an effective single-band summation

$$\begin{aligned} \sum_{n,m \neq n} \rho_{nm;L}^B(\omega) \mathcal{R}_{mn}^a e^{i\omega t} &= B_0^d e^{i\omega t} \frac{e}{4\hbar} \left[\sum_{n,m \neq n} g_{nm}^\omega [\epsilon_{dbc}(\partial_b f_n) v_{nm}^c] \mathcal{R}_{mn}^a + \sum_{n,m \neq n} (g_{nm}^{-\omega})^* [\epsilon_{dbc}(\partial_b f_n) v_{mn}^c] \mathcal{R}_{nm}^a \right] \\ &\quad - B_0^d e^{i\omega t} \frac{i}{2\hbar} \sum_{n,m \neq n} g_{mn}^\omega \left[-\frac{e}{2} \sum_{p \neq n} (\mathbf{v}_{mp} + \delta_{mp} \mathbf{v}_n) \times \mathcal{R}_{pn} \right]^d \mathcal{R}_{nm}^a (f_n - f_p) \\ &\quad + B_0^d e^{i\omega t} \frac{i}{2\hbar} \sum_{n,m \neq n} (g_{mn}^{-\omega})^* \left[-\frac{e}{2} \sum_{p \neq n} (\mathbf{v}_{pm} + \delta_{pm} \mathbf{v}_n) \times \mathcal{R}_{np} \right]^d \mathcal{R}_{mn}^a (f_n - f_p) . \end{aligned} \quad (\text{B15})$$

Simplifying a bit, we can express the above equation as,

$$\sum_{n,m \neq n} \rho_{nm;L}^B(\omega) \mathcal{R}_{mn}^a e^{i\omega t} = \sum_n f_n \left[\left(\mathcal{G}_{n\mathbf{k};L}^{B;ad}(\omega) + [\mathcal{G}_{n\mathbf{k};L}^{B;ad}(-\omega)]^* \right) B_0^d e^{i\omega t} \right] , \quad (\text{B16})$$

where we have defined,

$$\mathcal{G}_{n\mathbf{k};L}^{B;ad}(\omega) = -\frac{e}{4\hbar} \sum_{m \neq n} \epsilon_{dbc} \partial_b (g_{nm}^\omega v_{nm}^c \mathcal{R}_{mn}^a) - \frac{i}{2\hbar} \sum_{m \neq n} g_{mn}^\omega \mathcal{M}_{mn}^{L;d} \mathcal{R}_{nm}^a + \frac{i}{2\hbar} \sum_{m \neq p} \sum_{p \neq n} g_{mp}^\omega \mathcal{M}_{mnp}^{L;d} \mathcal{R}_{pm}^a . \quad (\text{B17})$$

Here, $\mathcal{M}_{mnp}^L = -(e/2)(\mathbf{v}_{mn} + \delta_{mn}\mathbf{v}_p) \times \mathcal{R}_{np}$, and $\mathcal{M}_{mn}^L = \sum_{p \neq n} \mathcal{M}_{mpn}^L$ is the matrix element of the electronic orbital magnetic moment operator. Substitution of the result from Eq. (B15) into Eq. (B13) yields,

$$\begin{aligned}
\sum_{n,m \neq n} \rho_{nm;L}^B(t) \mathcal{R}_{mn}^a &= \sum_n f_n \left[\left(\mathcal{G}_{n\mathbf{k};L}^{B;ad}(\omega) + [\mathcal{G}_{n\mathbf{k};L}^{B;ad}(-\omega)]^* \right) B_0^d e^{i\omega t} \right] + (\omega \rightarrow -\omega) , \\
&= \sum_n f_n \left[\left(\mathcal{G}_{n\mathbf{k};L}^{B;ad}(\omega) + [\mathcal{G}_{n\mathbf{k};L}^{B;ad}(-\omega)]^* \right) B_0^d e^{i\omega t} + \text{c.c.} \right] \\
&= \sum_n f_n \left[\tilde{\mathcal{G}}_{n\mathbf{k};L}^{B;ad}(\omega) B_0^d e^{i\omega t} + \text{c.c.} \right] \\
&= \sum_n f_n \mathcal{R}_{n\mathbf{k};L}^{B;a}(t) .
\end{aligned} \tag{B18}$$

In the final line of Eq. (B18), we expressed the density matrix trace of the unperturbed Berry connection as a single band sum of a band geometric quantity $\mathcal{R}_{n\mathbf{k};L}^{B;a}(t)$ weighted by the equilibrium Fermi function. This quantity can be interpreted as the orbital part of the magnetic field induced Berry connection correction,

$$\mathcal{R}_{n\mathbf{k};L}^{B;a}(t) = \tilde{\mathcal{G}}_{n\mathbf{k};L}^{B;ad}(\omega) B_0^d e^{i\omega t} + \text{c.c.} , \tag{B19}$$

where, we defined a band-geometric quantity *orbital*-Magnetic Berry connection polarizability (*orbital*-MBCP) $\tilde{\mathcal{G}}_{n\mathbf{k};L}^{B;ad}(\omega)$. Its expression is given by,

$$\tilde{\mathcal{G}}_{n\mathbf{k};L}^{B;ad}(\omega) = \mathcal{G}_{n\mathbf{k};L}^{B;ad}(\omega) + [\mathcal{G}_{n\mathbf{k};L}^{B;ad}(-\omega)]^* . \tag{B20}$$

b. Spin part of the Berry connection correction

The spin part of the magnetic field driven Berry connection correction can be obtained by evaluating the effective single band expression of the term,

$$\sum_{n,m \neq n} \rho_{nm;S}^B(t) \mathcal{R}_{mn}^a = \sum_{n,m \neq n} \rho_{nm;S}^B(\omega) \mathcal{R}_{mn}^a e^{i\omega t} + (\omega \rightarrow -\omega) . \tag{B21}$$

We substitute the density matrix expression from Eq. (A13) to obtain

$$\begin{aligned}
\sum_{n,m \neq n} \rho_{nm;S}^B(\omega) \mathcal{R}_{mn}^a &= \frac{i\mathbf{g}_s \mu_B}{4\hbar} \sum_{n,m \neq n} g_{nm}^\omega e^{i\omega t} [\mathbf{B}_0 \cdot \boldsymbol{\sigma}_{nm}] \mathcal{R}_{mn}^a f_{nm} \\
&= \frac{i\mathbf{g}_s \mu_B}{4\hbar} \sum_{n,m \neq n} e^{i\omega t} \mathbf{B}_0 \cdot [f_n g_{nm}^\omega \boldsymbol{\sigma}_{nm} \mathcal{R}_{mn}^a - f_m g_{nm}^\omega \boldsymbol{\sigma}_{nm} \mathcal{R}_{mn}^a] .
\end{aligned} \tag{B22}$$

Interchanging the dummy indices ($m \leftrightarrow n$) for the second term results in,

$$\begin{aligned}
\sum_{n,m \neq n} \rho_{nm;S}^B(\omega) \mathcal{R}_{mn}^a &= \frac{i\mathbf{g}_s \mu_B}{4\hbar} \sum_{n,m \neq n} e^{i\omega t} \mathbf{B}_0 \cdot [f_n g_{nm}^\omega \boldsymbol{\sigma}_{nm} \mathcal{R}_{mn}^a - f_n g_{mn}^\omega \boldsymbol{\sigma}_{mn} \mathcal{R}_{nm}^a] \\
&= \frac{i\mathbf{g}_s \mu_B}{4\hbar} \sum_{n,m \neq n} e^{i\omega t} \mathbf{B}_0 \cdot [f_n g_{nm}^\omega \boldsymbol{\sigma}_{nm} \mathcal{R}_{mn}^a - f_n (g_{nm}^{-\omega})^* \boldsymbol{\sigma}_{mn} \mathcal{R}_{nm}^a] .
\end{aligned} \tag{B23}$$

Substitution of the result from Eq. (B23) into Eq. (B21) results in

$$\begin{aligned}
\sum_{n,m \neq n} \rho_{nm;S}^B(t) \mathcal{R}_{mn}^a &= \sum_{n,m \neq n} \rho_{nm;S}^B(\omega) \mathcal{R}_{mn}^a e^{i\omega t} + (\omega \rightarrow -\omega) \\
&= \frac{i g_s \mu_B}{4\hbar} \sum_{n,m \neq n} e^{i\omega t} \mathbf{B}_0 \cdot [f_n g_{nm}^\omega \boldsymbol{\sigma}_{nm} \mathcal{R}_{mn}^a - f_n (g_{nm}^{-\omega})^* \boldsymbol{\sigma}_{mn} \mathcal{R}_{nm}^a] + (\omega \rightarrow -\omega) \\
&= \frac{i}{2\hbar} \sum_n f_n \sum_{m \neq n} \cdot [g_{mn}^\omega \mathcal{M}_{mn}^{S;d} \mathcal{R}_{nm}^a - (g_{mn}^{-\omega})^* \mathcal{M}_{nm}^{S;d} \mathcal{R}_{mn}^a] B_0^d e^{i\omega t} + \text{c.c.} \\
&= \sum_n f_n [\mathcal{G}_{n\mathbf{k};S}^{B;ad}(\omega) + [\mathcal{G}_{n\mathbf{k};S}^{B;ad}(-\omega)]^*] B_0^d e^{i\omega t} + \text{c.c.} \\
&= \sum_n f_n [\tilde{\mathcal{G}}_{n\mathbf{k};S}^{B;ad}(\omega) B_0^d e^{i\omega t} + \text{c.c.}] \\
&= \sum_n f_n \mathcal{R}_{n\mathbf{k};S}^{B;a}(t) .
\end{aligned} \tag{B24}$$

To obtain the expression in the third line of the above equation, we have used the relation $(g_{nm}^{-\omega})^* = g_{mn}^\omega$. Here,

$$\mathcal{R}_{n\mathbf{k};S}^{B;a}(t) = \tilde{\mathcal{G}}_{n\mathbf{k};S}^{B;ad}(\omega) B_0^d e^{i\omega t} + \text{c.c.} \tag{B25}$$

corresponds to the spin part of the magnetic field induced Berry connection correction. It is related to the *spin*-MBCP tensor

$$\tilde{\mathcal{G}}_{n\mathbf{k};S}^{B;ad} = \mathcal{G}_{n\mathbf{k};S}^{B;ad}(\omega) + [\mathcal{G}_{n\mathbf{k};S}^{B;ad}(-\omega)]^*, \tag{B26}$$

where

$$\mathcal{G}_{n\mathbf{k};S}^{B;ad}(\omega) = \frac{i}{2\hbar} \sum_{m \neq n} g_{mn}^\omega \mathcal{M}_{mn}^{S;d} \mathcal{R}_{nm}^a. \tag{B27}$$

The matrix element of the spin magnetic moment $\mathcal{M}_{mn}^{S;d} = -(g_s \mu_B/2) \sigma_{mn}^d$.

Now, we combine the results of orbital and spin contributions to write the total magnetic field induced Berry connection correction,

$$\mathcal{R}_{n\mathbf{k}}^{B;a}(t) = \mathcal{R}_{n\mathbf{k};L}^{B;a}(t) + \mathcal{R}_{n\mathbf{k};S}^{B;a}(t) = \tilde{\mathcal{G}}_{n\mathbf{k}}^{B;ad}(\omega) B_0^d e^{i\omega t} + \text{c.c.} \tag{B28}$$

Here,

$$\tilde{\mathcal{G}}_{n\mathbf{k}}^{B;ad}(\omega) = \tilde{\mathcal{G}}_{n\mathbf{k};L}^{B;ad}(\omega) + \tilde{\mathcal{G}}_{n\mathbf{k};S}^{B;ad}(\omega), \tag{B29}$$

and expressions of $\tilde{\mathcal{G}}_{n\mathbf{k};L}^{B;ad}(\omega)$ and $\tilde{\mathcal{G}}_{n\mathbf{k};S}^{B;ad}(\omega)$ are given in Eqs. (B20) and (B26), respectively.

c. Zero frequency result of the Berry connection correction

In the transport regime ($\omega\tau \ll 1$) for a dc magnetic field ($\omega = 0$), the Berry connection correction can be split into an intrinsic and extrinsic part. This can be done by approximating the scattering time-dependent g_{nm}^ω term as

$$g_{nm}(\omega = 0) = \frac{1}{\frac{1}{\tau} + i\omega_{nm}} \approx -\frac{i}{\omega_{nm}} + \frac{1}{\omega_{nm}^2 \tau}. \tag{B30}$$

For typical topological materials, the scattering time is $\tau \sim 1 \text{ ps}$ ^{66,67}, corresponding to an energy scale $\hbar/\tau \sim 0.7 \text{ meV}$. By contrast, in gapped systems, and in gapless systems away from band-touching points, the relevant interband energy scale is typically $\hbar\omega_{nm} \sim 100 \text{ meV}$ ^{16,59,62,68}. Consequently, $\omega_{nm}\tau \gg 1$, and the subleading term in the above expansion can be neglected. Keeping only the leading contribution gives $g_{nm}(\omega = 0) \simeq -i/\omega_{nm}$, and substituting this approximation into Eq. (B28) yields the magnetic field induced intrinsic Berry-connection correction

$$\tilde{\mathcal{R}}_{nn}^{B;a} = -2 \operatorname{Re} \sum_{m \neq n} \frac{\mathcal{R}_{nm}^a [\mathbf{B} \cdot (\mathcal{M}_{mn}^L - \mathcal{M}_{mn}^S)]}{\varepsilon_m - \varepsilon_n} - \frac{e}{\hbar} B^d \epsilon_{dbc} (\partial_b g_n^{ca}) - 2 \operatorname{Re} \left[\sum_{m \neq p} \sum_{p \neq n} \frac{\mathcal{R}_{pm}^a (\mathbf{B} \cdot \mathcal{M}_{mnp}^L)}{\varepsilon_p - \varepsilon_m} \right], \tag{B31}$$

where $g_n^{ca} = \sum_{m \neq n} \text{Re}(\mathcal{R}_{nm}^c \mathcal{R}_{mn}^a)$ is the quantum metric tensor. The last term represents a novel multiband correction to the existing semiclassical expression.

Appendix C: Equations of motion

In this section, we aim to derive the equations of motion of Bloch electrons. The dynamics of the charge carriers are governed by the Euler-Lagrange equations

$$\frac{d}{dt} \left(\frac{\partial \mathcal{L}_{n\mathbf{k}}}{\partial \dot{\mathbf{r}}_n} \right) = \frac{\partial \mathcal{L}_{n\mathbf{k}}}{\partial \mathbf{r}_n}, \quad (\text{C1})$$

$$\frac{d}{dt} \left(\frac{\partial \mathcal{L}_{n\mathbf{k}}}{\partial \dot{\mathbf{k}}} \right) = \frac{\partial \mathcal{L}_{n\mathbf{k}}}{\partial \mathbf{k}}. \quad (\text{C2})$$

For convenience, we write the Lagrangian expression derived in Eq. (B11)

$$\mathcal{L}_{n\mathbf{k}} = -\hbar \dot{\mathbf{k}} \cdot \left[\mathbf{r}_n - \left(\mathcal{R}_{n\mathbf{k}} + \mathcal{R}_{n\mathbf{k}}^B(t) \right) \right] + \frac{e}{2} [\mathbf{B}(t) \times \dot{\mathbf{r}}_n] \cdot \mathbf{r}_n - \tilde{\varepsilon}_{n\mathbf{k}}. \quad (\text{C3})$$

The first Euler-Lagrange equation yields the force equation,

$$\begin{aligned} \frac{e}{2} [\dot{\mathbf{r}}_n \times \mathbf{B}(t)] &= -\hbar \dot{\mathbf{k}} + \frac{e}{2} [\mathbf{B}(t) \times \dot{\mathbf{r}}_n] \\ \Rightarrow \hbar \dot{\mathbf{k}} &= -e [\dot{\mathbf{r}}_n \times \mathbf{B}(t)], \end{aligned} \quad (\text{C4})$$

The second Euler-Lagrange equation produces the velocity equation of the charge particle,

$$\begin{aligned} \frac{d\mathbf{r}_n^a}{dt} &= \frac{1}{\hbar} \frac{\partial \tilde{\varepsilon}_{n\mathbf{k}}}{\partial k_a} + \left(\frac{d\mathcal{R}_{n\mathbf{k}}^a}{dt} + \frac{d\mathcal{R}_{n\mathbf{k}}^{B;a}}{dt} \right) - \frac{\partial}{\partial k_a} \left[\dot{\mathbf{k}} \cdot \left(\mathcal{R}_{n\mathbf{k}} + \mathcal{R}_{n\mathbf{k}}^B(t) \right) \right] \\ \Rightarrow \dot{\mathbf{r}}_n^a &= \tilde{v}_{n\mathbf{k}}^a + \left(\dot{\mathbf{k}} \cdot \frac{\partial \mathcal{R}_{nn}^a}{\partial \mathbf{k}} - \dot{\mathbf{k}} \cdot \frac{\partial \mathcal{R}_{n\mathbf{k}}}{\partial k_a} \right) + \left(\dot{\mathbf{k}} \cdot \frac{\partial \mathcal{R}_{n\mathbf{k}}^{B;a}}{\partial \mathbf{k}} - \dot{\mathbf{k}} \cdot \frac{\partial \mathcal{R}_{n\mathbf{k}}^B}{\partial k_a} \right) + \frac{\partial \mathcal{R}_{n\mathbf{k}}^{B;a}}{\partial t} \\ &= \tilde{v}_{n\mathbf{k}}^a - [\dot{\mathbf{k}} \times (\boldsymbol{\Omega}_{n\mathbf{k}} + \boldsymbol{\Omega}_{n\mathbf{k}}^B)]^a + \frac{\partial \mathcal{R}_{n\mathbf{k}}^{B;a}}{\partial t}. \end{aligned} \quad (\text{C5})$$

Here, $\tilde{v}_{n\mathbf{k}}^a$ is the magnetic field corrected band velocity and $\boldsymbol{\Omega}_{n\mathbf{k}}(\boldsymbol{\Omega}_{n\mathbf{k}}^B) = \partial_{\mathbf{k}} \times \mathcal{R}_{n\mathbf{k}}(\mathcal{R}_{n\mathbf{k}}^B)$ is the intrinsic (magnetic field induced) Berry curvature of the system. The second term produces an anomalous velocity of the charge carrier. The third term is a consequence of an oscillating magnetic field and would vanish in the dc limit. The gyrotropic current due to the spin part of the oscillating Berry connection has been demonstrated in a recent article by Jian Wang *et al.*²³. Recently, a similar velocity component has been discovered in case of an oscillating electric field, yielding the electric displacement current²¹, and quantum capacitance in insulators²². Eqs. (C4) and (C5) can be decoupled and written in the following form

$$\dot{\mathbf{r}}_{n\mathbf{k}} = D_{n\mathbf{k}} \left[\tilde{v}_{n\mathbf{k}} + \frac{e}{\hbar} (\tilde{v}_{n\mathbf{k}} \cdot \tilde{\boldsymbol{\Omega}}_{n\mathbf{k}}) \mathbf{B} + \frac{\partial \mathcal{R}_{n\mathbf{k}}^B}{\partial t} + \frac{e}{\hbar} \left(\frac{\partial \mathcal{R}_{n\mathbf{k}}^B}{\partial t} \cdot \tilde{\boldsymbol{\Omega}}_{n\mathbf{k}} \right) \mathbf{B} \right], \quad (\text{C6})$$

$$\hbar \dot{\mathbf{k}} = D_{n\mathbf{k}} \left[-e (\tilde{v}_{n\mathbf{k}} \times \mathbf{B}) - e \left(\frac{\partial \mathcal{R}_{n\mathbf{k}}^B}{\partial t} \times \mathbf{B} \right) \right], \quad (\text{C7})$$

where $\tilde{\boldsymbol{\Omega}}_{n\mathbf{k}} = (\boldsymbol{\Omega}_{n\mathbf{k}} + \boldsymbol{\Omega}_{n\mathbf{k}}^B)$ is total Berry curvature.

Appendix D: Intrinsic gyrotropic magnetic current

In the last section, we derived the particle velocity in the presence of an oscillating magnetic field. This velocity weighted by the momentum space equilibrium Fermi function yields the intrinsic charge current,

$$\mathbf{j} = -e \int_{n\mathbf{k}} D_{n\mathbf{k}}^{-1} \dot{\mathbf{r}}_{n\mathbf{k}} f_{n\mathbf{k}}, \quad (\text{D1})$$

where, we have defined $\int_{n\mathbf{k}} \equiv \sum_n d^d \mathbf{k} / (2\pi)^d$, d is the spatial dimension. Substitution of the result from Eq. (C6) into the above equation and keeping terms only up to first order in the magnetic field, we obtain the linear charge current to be

$$\mathbf{j} = -e \int_{n\mathbf{k}} \left[\mathbf{v}_{n\mathbf{k}}^B + \frac{e}{\hbar} (\mathbf{v}_{n\mathbf{k}} \cdot \boldsymbol{\Omega}_{n\mathbf{k}}) \mathbf{B} + \frac{\partial \mathcal{R}_{n\mathbf{k}}^B}{\partial t} \right] f_{n\mathbf{k}} . \quad (\text{D2})$$

Now, as shown in the main text, the oscillating magnetic field induced linear charge current can be written as

$$j_a^{\text{GMC}}(t) = \chi_{a;d}^{\text{GMC}}(\omega) B_0^d e^{i\omega t} + \text{c.c.} \quad (\text{D3})$$

Here, $\chi_{a;d}^{\text{GMC}}(\omega)$ is the gyrotropic magnetic conductivity for the current flowing along a -axis with the field along d -axis. Depending on physical origins, the response tensor $\chi_{a;d}^{\text{GMC}}(\omega)$ can be decomposed into three different parts, which are Fermi surface oscillation (FO), chiral magnetic velocity (CMV), and dynamic charge polarization, denoted as displacement current (Disp), i.e.,

$$\chi_{a;d}^{\text{GMC}}(\omega) = \chi_{a;d}^{\text{G,FO}} + \chi_{a;d}^{\text{G,Disp}} + \chi_{a;d}^{\text{G,CMV}} . \quad (\text{D4})$$

The explicit expressions of $\chi_{a;d}^{\text{G,FO}}(\omega)$, $\chi_{a;d}^{\text{G,CMV}}(\omega)$, and $\chi_{a;d}^{\text{G,Disp}}(\omega)$ are

$$\chi_{a;d}^{\text{G,FO}}(\omega) = -ie\omega g_0^\omega \int_{n\mathbf{k}} v_{n\mathbf{k}}^a \mathcal{M}_{n\mathbf{k}}^d \frac{\partial f_{n\mathbf{k}}}{\partial \varepsilon_{n\mathbf{k}}} , \quad (\text{D5})$$

$$\chi_{a;d}^{\text{G,Disp}}(\omega) = -ie\omega \int_{n\mathbf{k}} \tilde{G}_{n\mathbf{k}}^{B;ad}(\omega) f_{n\mathbf{k}} , \quad (\text{D6})$$

$$\chi_{a;d}^{\text{G,CMV}}(\omega) = -\frac{e^2}{\hbar} \delta_{ad} \int_{n\mathbf{k}} (\mathbf{v}_{n\mathbf{k}} \cdot \boldsymbol{\Omega}_{n\mathbf{k}}) f_{n\mathbf{k}} . \quad (\text{D7})$$

From Eq. (D7), it is clear that the chiral magnetic velocity contribution is purely intrinsic and driven by the Berry curvature of the system. But, the other two contributions of GMC, namely the conventional Fermi surface term and the displacement currents, depend on the scattering time τ . Their τ dependence originate from the factors $g_0^\omega = [1/\tau + i\omega]^{-1}$ and $g_{nm}^\omega = [1/\tau + i(\omega_{nm} + \omega)]^{-1}$. These factors can be expanded binomially, and based on the relative magnitudes of the scattering time, driving frequency and characteristic interband transition frequency, they can be segregated into an intrinsic and extrinsic part. Here, we work in the transport regime, where $\omega\tau \ll 1$. In this limit, these factors approximate as $g_0^\omega \approx \tau$ and $g_{nm}^\omega \approx -i/\omega_{nm}$ [See Eq. (B30)]. Substituting these results into Eqs. (D5) and (D6) yields the conventional GMC to be purely extrinsic and the displacement contribution a purely intrinsic response. Thereby, the intrinsic gyrotropic magnetic current (IGMC) is given by

$$\chi_{a;d}^{\text{IGMC}}(\omega) = \chi_{a;d}^{\text{IG,Disp}} + \chi_{a;d}^{\text{IG,CMV}} . \quad (\text{D8})$$

Here, the displacement contribution of IGMC depends on the intrinsic part of the MBCP tensor in the transport regime, given by

$$\tilde{G}_{n\mathbf{k};L/S}^{B;ad} = \lim_{\omega \ll 1/\tau} \tilde{G}_{n\mathbf{k};L/S}^{B;ad}(\omega) = G_{n\mathbf{k};L/S}^{B;ad} + [G_{n\mathbf{k};L/S}^{B;ad}]^* , \quad (\text{D9})$$

where

$$G_{n\mathbf{k};L}^{B;ad} = -\frac{e}{2\hbar} \sum_{m \neq n} \epsilon_{dbc} (\partial_b G_n^{ca}) - \text{Re} \sum_{m \neq n} \frac{\mathcal{M}_{mn}^{L;d} \mathcal{R}_{nm}^a}{\varepsilon_m - \varepsilon_n} + \text{Re} \sum_{m \neq p} \sum_{p \neq n} \frac{\mathcal{M}_{mnp}^{L;d} \mathcal{R}_{pm}^a}{\varepsilon_m - \varepsilon_p} , \quad (\text{D10})$$

$$\tilde{G}_{n\mathbf{k};S}^{B;ad} = \text{Re} \sum_{m \neq n} \frac{\mathcal{M}_{mn}^{S;d} \mathcal{R}_{nm}^a}{\varepsilon_m - \varepsilon_n} . \quad (\text{D11})$$

Importantly, in the low frequency regime, the driving frequency being much lower compared to the system's interband frequency, the band geometric MBCP tensors become independent of the driving frequency and coincide with the zero frequency result [see Eq. (B31)].

Appendix E: Magnetic point group symmetry of the IGMC tensors

The IGMC response tensor can be segregated into \mathcal{T} -even and \mathcal{T} -odd parts based on the time-reversal parity of the corresponding conductivity expressions. A microscopic symmetry analysis of the two contributing channels: displacement current and chiral magnetic velocity, shows that $\chi_{a;d}^{\text{IG,CMV}}$ is \mathcal{T} -even and can therefore be finite in both magnetic and nonmagnetic systems. In contrast, the displacement contribution $\chi_{a;d}^{\text{IG,Disp}}$ is \mathcal{T} -odd and vanishes in nonmagnetic materials. To assess the feasibility of these contributions for nonmagnetic systems, we presented the crystallographic point group analysis in Table III of Sec. IV. We now complete the symmetry classification by examining the symmetry for magnetic point groups. Notably, the symmetry tables reveal that both these contributions vanish identically in systems possessing $\mathcal{C}_{3,4,6}^z \mathcal{T}$ symmetry, or equivalently pure rotational symmetries $\mathcal{C}_{2,3,4,6}^z$.

TABLE IV. The symmetry restrictions of the magnetic gyrotropic response tensors. The cross (\times) and the tick (\checkmark) mark signify that the corresponding response tensor is symmetry forbidden and allowed, respectively. Here, \mathcal{M}_a , \mathcal{C}_n^a and \mathcal{S}_n^a represent mirror, n -fold rotation, and n -fold roto-reflection symmetry operation along the a -direction for $a = \{x, y, z\}$, respectively.

IGMC	$\mathcal{M}_x \mathcal{T}$	$\mathcal{M}_y \mathcal{T}$	$\mathcal{M}_z \mathcal{T}$	$\mathcal{C}_2^x \mathcal{T}$	$\mathcal{C}_2^y \mathcal{T}$	$\mathcal{C}_2^z \mathcal{T}$	$\mathcal{C}_4^x \mathcal{T}$	$\mathcal{C}_4^y \mathcal{T}$	$\mathcal{C}_{3,6}^x \mathcal{T}$	$\mathcal{C}_{3,6}^y \mathcal{T}$	$\mathcal{C}_{3,4,6}^z \mathcal{T}$	$\mathcal{S}_4^x \mathcal{T}$	$\mathcal{S}_6^x \mathcal{T}$	$\mathcal{S}_4^y \mathcal{T}$	$\mathcal{S}_6^y \mathcal{T}$	$\mathcal{S}_{4,6}^z \mathcal{T}$
$\chi_{x;z}^{\text{IG,Disp}}$	\times	\checkmark	\times	\checkmark	\times	\checkmark	\times	\checkmark	\times	\times	\times	\times	\times	\times	\checkmark	\checkmark
$\chi_{y;z}^{\text{IG,Disp}}$	\checkmark	\times	\times	\times	\checkmark	\checkmark	\checkmark	\times	\times	\times	\times	\checkmark	\checkmark	\times	\times	\times
$\chi_{x;z}^{\text{IG,CMV}}$	\checkmark	\times	\checkmark	\times	\checkmark	\times	\times	\checkmark	\times	\checkmark	\times	\times	\times	\checkmark	\times	\times
$\chi_{y;z}^{\text{IG,CMV}}$	\times	\checkmark	\checkmark	\checkmark	\times	\times	\checkmark	\times	\checkmark	\times	\checkmark	\checkmark	\times	\times	\times	\times

* koushikgh20@iitk.ac.in

† sankars24@iitk.ac.in

‡ amitag@iitk.ac.in

¹ Lev Davidovich Landau, John Stewart Bell, MJ Kearsley, LP Pitaevskii, EM Lifshitz, and JB Sykes, *Electrodynamics of continuous media*, Vol. 8 (elsevier, 2013).

² Yu I Krasilov, VI Burkov, *et al.*, “Experimental studies of gyrotropy of crystals,” *Soviet Physics Uspekhi* **17**, 745 (1975).

³ Shudan Zhong, Joseph Orenstein, and Joel E. Moore, “Optical gyrotropy from axion electrodynamics in momentum space,” *Phys. Rev. Lett.* **115**, 117403 (2015).

⁴ Pavan Hosur and Xiao-Liang Qi, “Tunable circular dichroism due to the chiral anomaly in weyl semimetals,” *Phys. Rev. B* **91**, 081106 (2015).

⁵ V.M. Asnin, A.A. Bakun, A.M. Danishevskii, E.L. Ivchenko, G.E. Pikus, and A.A. Rogachev, ““circular” photogalvanic effect in optically active crystals,” *Solid State Communications* **30**, 565–570 (1979).

⁶ Wen-Yu He and K. T. Law, “Magnetoelectric effects in gyrotropic superconductors,” *Phys. Rev. Res.* **2**, 012073 (2020).

⁷ Fabian Jäger, Nicola A. Spaldin, and Sayantika Bhowal, “Universal responses in nonmagnetic polar metals,” *Phys. Rev. Res.* **6**, 013251 (2024).

⁸ Sayan Sarkar, Sunit Das, Debottam Mandal, and Amit Agarwal, “Light-induced nonlinear resonant spin magnetization,” *New Journal of Physics* **27**, 113503 (2025).

⁹ E. J. König, M. Dzero, A. Levchenko, and D. A. Pesin, “Gyrotropic hall effect in berry-curved materials,” *Phys. Rev. B* **99**, 155404 (2019).

¹⁰ Shudan Zhong, Joel E. Moore, and Ivo Souza, “Gyrotropic magnetic effect and the magnetic moment on the fermi surface,” *Phys. Rev. Lett.* **116**, 077201 (2016).

¹¹ Pallab Goswami, Gargee Sharma, and Sumanta Tewari, “Optical activity as a test for dynamic chiral magnetic effect of weyl semimetals,” *Phys. Rev. B* **92**, 161110 (2015).

¹² Nisarga Paul, Takamori Park, Jung Hoon Han, and Leon Balents, “Gyrotropic magnetic effect in metallic chiral magnets,” *Phys. Rev. Lett.* **135**, 246704 (2025).

¹³ Urmimala Dey, S Nandy, and A Taraphder, “Dynamic chiral magnetic effect and anisotropic natural optical activity of tilted weyl semimetals,” *Scientific Reports* **10**, 2699 (2020).

¹⁴ Rhonald Burgos Atencia, Amit Agarwal, and Dimitrie Culcer, “Orbital angular momentum of bloch electrons: equilibrium formulation, magneto-electric phenomena, and the orbital hall effect,” *Advances in Physics: X* **9**, 2371972 (2024).

¹⁵ Felix Flicker, Fernando de Juan, Barry Bradlyn, Takahiro Morimoto, Maia G. Vergniory, and Adolfo G. Grushin, “Chiral optical response of multifold fermions,” *Phys. Rev. B* **98**, 155145 (2018).

¹⁶ Subhajit Sinha, Pratap Chandra Adak, Atasi Chakraborty, Kamal Das, Koyendrila Debnath, LD Varma Sangani, Kenji Watanabe, Takashi Taniguchi, Umesh V Waghmare, Amit Agarwal, *et al.*, “Berry curvature dipole senses topological transition in a moiré superlattice,” *Nature Physics* **18**, 765–770 (2022).

¹⁷ Atasi Chakraborty, Kamal Das, Subhajit Sinha, Pratap Chandra Adak, Mandar M Deshmukh, and Amit Agarwal, “Nonlinear anomalous hall effects probe topological phase-transitions in twisted double bilayer

graphene,” *2D Materials* **9**, 045020 (2022).

¹⁸ J. Rou, C. Şahin, J. Ma, and D. A. Pesin, “Kinetic orbital moments and nonlocal transport in disordered metals with nontrivial band geometry,” *Phys. Rev. B* **96**, 035120 (2017).

¹⁹ Yang Gao, Shengyuan A. Yang, and Qian Niu, “Field induced positional shift of bloch electrons and its dynamical implications,” *Phys. Rev. Lett.* **112**, 166601 (2014).

²⁰ Yang Gao, “Semiclassical dynamics and nonlinear charge current,” *Frontiers of Physics* **14**, 33404 (2019).

²¹ Jinxiong Jia, Longjun Xiang, Zhenhua Qiao, and Jian Wang, “Equivalence of semiclassical and response theories for second-order nonlinear ac hall effects,” *Phys. Rev. B* **110**, 245406 (2024).

²² Ilia Komissarov, Tobias Holder, and Raquel Queiroz, “The quantum geometric origin of capacitance in insulators,” *Nature communications* **15**, 4621 (2024).

²³ Longjun Xiang, Jinxiong Jia, Fuming Xu, Zhenhua Qiao, and Jian Wang, “Intrinsic gyroscopic magnetic current from zeeman quantum geometry,” *Phys. Rev. Lett.* **134**, 116301 (2025).

²⁴ Young-Gwan Choi, Daegeun Jo, Kyung-Hun Ko, Dongwook Go, Kyung-Han Kim, Hee Gyum Park, Changyoung Kim, Byoung-Chul Min, Gyung-Min Choi, and Hyun-Woo Lee, “Observation of the orbital hall effect in a light metal ti,” *Nature* **619**, 52–56 (2023).

²⁵ Igor Lyalin, Sanaz Alikhah, Marco Berritta, Peter M. Oppeneer, and Roland K. Kawakami, “Magneto-optical detection of the orbital hall effect in chromium,” *Phys. Rev. Lett.* **131**, 156702 (2023).

²⁶ Giacomo Sala, Hanchen Wang, William Legrand, and Pietro Gambardella, “Orbital hanle magnetoresistance in a 3d transition metal,” *Phys. Rev. Lett.* **131**, 156703 (2023).

²⁷ Ryoga Matsumoto, Ryo Ohshima, Yuichiro Ando, Dongwook Go, Yuriy Mokrousov, and Masashi Shiraishi, “Observation of giant orbital hall effect in si,” *arXiv preprint arXiv:2501.14237* (2025).

²⁸ Koushik Ghorai, Sunit Das, Harsh Varshney, and Amit Agarwal, “Planar hall effect in quasi-two-dimensional materials,” *Phys. Rev. Lett.* **134**, 026301 (2025).

²⁹ Kazuki Nakazawa, Terufumi Yamaguchi, and Ai Yamakage, “Orbital-related gyroscopic responses in Cu₂WSe₄ and chirality indicator,” (2025), *arXiv:2512.16387* [cond-mat.mtrl-sci].

³⁰ Fan Yang, Xu-Tao Zeng, Huiying Liu, Cong Xiao, Xian-Lei Sheng, and Shengyuan A. Yang, “Orbital-dominated intrinsic nonlinear planar hall response and its application in CuTlSe₂,” *Phys. Rev. B* **112**, 245153 (2025).

³¹ Rahul Biswas, Harsh Varshney, and Amit Agarwal, “Planar nernst effect from hidden band geometry in layered two-dimensional materials,” *Phys. Rev. B* **112**, 075420 (2025).

³² Kamal Das and Amit Agarwal, “Intrinsic hall conductivities induced by the orbital magnetic moment,” *Phys. Rev. B* **103**, 125432 (2021).

³³ Sunit Das, Akash Adhikary, Divya Sahani, Aveek Bid, and Amit Agarwal, “Odd-parity longitudinal magnetoconductivity in time-reversal symmetry broken materials,” *Phys. Rev. B* **113**, 035408 (2026).

³⁴ Zesheng Zhang, Xin-Zhi Li, and Wen-Yu He, “Orbital magnetization as the origin of the nonlinear hall effect,” *Phys. Rev. Res.* **7**, L042064 (2025).

³⁵ Chao Chen Ye, Karma Tenzin, Jagoda Sławińska, and Carmine Autieri, “Dominant orbital magnetization in the prototypical altermagnet mnte,” *arXiv preprint arXiv:2505.08675* (2025).

³⁶ Ganesh Sundaram and Qian Niu, “Wave-packet dynamics in slowly perturbed crystals: Gradient corrections and berry-phase effects,” *Phys. Rev. B* **59**, 14915–14925 (1999).

³⁷ Robert W. Boyd, *Nonlinear Optics*, 4th ed. (Academic Press, London, UK, 2020).

³⁸ Akihiko Sekine, Dimitrie Culcer, and Allan H. MacDonald, “Quantum kinetic theory of the chiral anomaly,” *Phys. Rev. B* **96**, 235134 (2017).

³⁹ Claudio Aversa and J. E. Sipe, “Nonlinear optical susceptibilities of semiconductors: Results with a length-gauge analysis,” *Phys. Rev. B* **52**, 14636–14645 (1995).

⁴⁰ Kamal Das, Shibalik Lahiri, Rhonald Burgos Atencia, Dimitrie Culcer, and Amit Agarwal, “Intrinsic nonlinear conductivities induced by the quantum metric,” *Phys. Rev. B* **108**, L201405 (2023).

⁴¹ Kamal Das, Koushik Ghorai, Dimitrie Culcer, and Amit Agarwal, “Nonlinear valley hall effect,” *Phys. Rev. Lett.* **132**, 096302 (2024).

⁴² Cong Xiao, Weikang Wu, Hui Wang, Yue-Xin Huang, Xiaolong Feng, Huiying Liu, Guang-Yu Guo, Qian Niu, and Shengyuan A. Yang, “Time-reversal-even nonlinear current induced spin polarization,” *Phys. Rev. Lett.* **130**, 166302 (2023).

⁴³ Neelanjan Chakraborti, Sudeep Kumar Ghosh, and Snehasish Nandy, “Zeeman quantum geometry as a probe of unconventional magnetism,” (2025), *arXiv:2508.14745* [cond-mat.mes-hall].

⁴⁴ Hui Wang, Yue-Xin Huang, Huiying Liu, Xiaolong Feng, Jiaoqiao Zhu, Weikang Wu, Cong Xiao, and Shengyuan A. Yang, “Orbital origin of the intrinsic planar hall effect,” *Phys. Rev. Lett.* **132**, 056301 (2024).

⁴⁵ Yang Gao, “Semiclassical dynamics and nonlinear charge current,” *Frontiers of Physics* **14**, 33404 (2019).

⁴⁶ Di Xiao, Junren Shi, and Qian Niu, “Berry phase correction to electron density of states in solids,” *Phys. Rev. Lett.* **95**, 137204 (2005).

⁴⁷ Tomoya Hayata, Yuta Kikuchi, and Yuya Tanizaki, “Topological properties of the chiral magnetic effect in multi-weyl semimetals,” *Phys. Rev. B* **96**, 085112 (2017).

⁴⁸ Sunit Das, Kamal Das, and Amit Agarwal, “Chiral anomalies in three-dimensional spin-orbit coupled metals: Electrical, thermal, and gravitational anomalies,” *Phys. Rev. B* **108**, 045405 (2023).

⁴⁹ D. T. Son and B. Z. Spivak, “Chiral anomaly and classical negative magnetoresistance of weyl metals,” *Phys. Rev. B* **88**, 104412 (2013).

⁵⁰ Kamal Das and Amit Agarwal, “Linear magnetochiral transport in tilted type-i and type-ii weyl semimetals,” *Phys. Rev. B* **99**, 085405 (2019).

⁵¹ Cong Xiao, Jin Cao, Qian Niu, and Shengyuan A. Yang, “Proper definition of intrinsic nonlinear current,” *Phys. Rev. Lett.* **135**, 256306 (2025).

⁵² Alexander Vilenkin, “Equilibrium parity-violating current in a magnetic field,” *Phys. Rev. D* **22**, 3080–3084 (1980).

⁵³ Kenji Fukushima, Dmitri E. Kharzeev, and Harmen J. Warringa, “Chiral magnetic effect,” *Phys. Rev. D* **78**, 074033 (2008).

⁵⁴ M. M. Vazifeh and M. Franz, “Electromagnetic response of weyl semimetals,” *Phys. Rev. Lett.* **111**, 027201 (2013).

⁵⁵ Naoki Yamamoto, “Generalized bloch theorem and chiral transport phenomena,” *Phys. Rev. D* **92**, 085011 (2015).

⁵⁶ Kamal Das and Amit Agarwal, “Thermal and gravitational chiral anomaly induced magneto-transport in weyl semimetals,” *Phys. Rev. Res.* **2**, 013088 (2020).

⁵⁷ Anmol Thakur, Krishanu Sadhukhan, and Amit Agarwal, “Dynamic current-current susceptibility in three-dimensional dirac and weyl semimetals,” *Phys. Rev. B* **97**, 035403 (2018).

⁵⁸ Robert E Newnham, *Properties of Materials: Anisotropy, Symmetry, Structure* (Oxford University Press, New York, 2005).

⁵⁹ L. Šmejkal, J. Železný, J. Sinova, and T. Jungwirth, “Electric control of dirac quasiparticles by spin-orbit torque in an antiferromagnet,” *Phys. Rev. Lett.* **118**, 106402 (2017).

⁶⁰ A Garrison Linn, Peipei Hao, Kyle N Gordon, Dushyant Narayan, Bryan S Berggren, Nathaniel Speiser, Sonka Reimers, Richard P Campion, Vít Novák, Sarnjeet S Dhesi, *et al.*, “Experimental electronic structure of the electrically switchable antiferromagnet cumnas,” *npj Quantum Materials* **8**, 19 (2023).

⁶¹ Hikaru Watanabe and Youichi Yanase, “Chiral photocurrent in parity-violating magnet and enhanced response in topological antiferromagnet,” *Phys. Rev. X* **11**, 011001 (2021).

⁶² Pankaj Bhalla, Kamal Das, Dimitrie Culcer, and Amit Agarwal, “Resonant second-harmonic generation as a probe of quantum geometry,” *Phys. Rev. Lett.* **129**, 227401 (2022).

⁶³ P Wadley, V Novák, RP Campion, Christian Rinaldi, X Martí, H Reichlová, J Železný, J Gazquez, MA Roldan, M Varela, *et al.*, “Tetragonal phase of epitaxial room-temperature antiferromagnet cumnas,” *Nature communications* **4**, 2322 (2013).

⁶⁴ David Wagenknecht, Karel Výborný, Karel Carva, and Ilja Turek, “Antiferromagnetic cumnas: Ab initio description of finite temperature magnetism and resistivity,” *Journal of Magnetism and Magnetic Materials* **513**, 167078 (2020).

⁶⁵ M. Mehraeen, “Quantum kinetic theory of quadratic responses,” *Phys. Rev. B* **110**, 174423 (2024).

⁶⁶ Da Ma, Arpit Arora, Giovanni Vignale, and Justin C. W. Song, “Anomalous skew-scattering nonlinear hall effect and chiral photocurrents in \mathcal{PT} -symmetric antiferromagnets,” *Phys. Rev. Lett.* **131**, 076601 (2023).

⁶⁷ ZZ Du, CM Wang, Shuai Li, Hai-Zhou Lu, and XC Xie, “Disorder-induced nonlinear hall effect with time-reversal symmetry,” *Nature Communications* **10**, 3047 (2019).

⁶⁸ Shuai Li, Tianyu Liu, Chang Liu, Yayu Wang, Hai-Zhou Lu, and X C Xie, “Progress on the antiferromagnetic topological insulator mnb₂te₄,” *National Science Review* **11**, nwac296 (2023).